$^{40}Ar/^{39}Ar$ laser-probe study of K-feldspars from the New Ross area of the South Mountain Batholith, Nova Scotia

Stephen N. Warren

Undergraduate Honours Thesis
Department of Earth Science
Dalhousie University
Halifax, Nova Scotia

Abstract

The peraluminous 372 Ma South Mountain Batholith (SMB) intruded the metasedimentary rocks of the Lower Paleozoic Meguma Supergroup in the Late Devonian. Within the New Ross Area of the SMB there are mineral concentrations. The laser-probe method was utilized on fragmented K-feldspar grains in order to investigate the low-temperature thermal history of the study areas as well as attempting to isolate the mineralization age of 372 Ma within the feldspar grain. Analyses are performed on four K-feldspar samples; two from Long Lake (mineralized greisen boulders and pegmatite), one from Walker Moly (pegmatite), and one from Millet Brook (mineralized fracture zone). Fragments of feldspar from these samples were completely outgassed by a Nd-YAG laser and the results were compared with previously obtained age spectra from the $^{40}Ar/^{39}Ar$ step-heating analysis of Long Lake, Walker Moly, and Millet Brook K-feldspars. Rims of the K-feldspar were separated from cores and analyzed for age variability in all samples except for those from Millet Brook. For the Long Lake mineralized greisen, a mean apparent age of 260.4 ± 2.8 Ma was calculated with the laser-probe with no rim/core age correlation. The Walker Moly pegmatite had a laser-probe calculated mean apparent age of 349.9 ± 3.2 Ma with no age variations based on rim/core data. The laser analysis of the Long Lake pegmatite yielded the largest scatter of fragment ages (279.5 ± 4.7 to 353.0 ± 6.3 Ma) with a mean age of 319.6 ± 3.0 Ma. The corresponding age spectrum for this sample is the most discordant of all analyzed samples, reflecting variability in the spatial distribution of radiogenic Ar within the K-feldspar grain. The mean apparent age determined by laser analysis for the Millet Brook K-feldspar sample was calculated to be 355.4 ± 3.5 Ma. The relatively low scatter in the plot of fragment ages (346.5 ± 4.8 to 363.4 ± 5.3 Ma) reflected the low range of ages on the age spectrum. Most likely, there has been some interplay of slow K-feldspar cooling, prolonged open system conditions, and partial resetting during the geological history. These areas had been completely exhumed by 355 Ma as this is the age determined for the base of the overlying Horton Group of sediments. The low mean of ca. 260 Ma for the mineralized greisen K-feldspar can be interpreted as the result of poor argon retention. An alternative interpretation relates to hydrothermal fluid interaction similar to events responsible of ca. 260 Ma ages determined in the southwest portion of the SMB. The degree to which the mineralogical features of these samples affect the obtained $^{40}Ar/^{39}Ar$ dates should be considered further if future studies are to be conducted.

Table of Contents

Table of Figures

Table of Tables

Acknowledgements

I would like to thank my thesis advisor Peter Reynolds. I am very grateful to Sarah Carruzzo for all the advice, thin section work, fieldwork, and support. Thanks to Keith Taylor for his technical expertise in the argon lab. The hand sample photographs are credited to Krista McCuish who spent a day with Sarah and I in search of samples. I greatly appreciate the help of D. B. Clarke for sharing his vast knowledge of potassium feldspars and the South Mountain Batholith, and for his assistance with the thin section observations. Marcos Zentilli and Martin Gibling must be acknowledged for all the helpful comments they gave me in the early drafts of this thesis and for the academic direction they have provided me. Thanks also to Dan Kontak for his many helpful suggestions.

Chapter 1: Introduction

1.1 General Statement

The peraluminous South Mountain Batholith (SMB) was intruded into the sedimentary rocks of the Meguma Supergroup in the Late Devonian. Within the batholith are several areas that were hydrothermally altered during its evolution. Associated with these hydrothermally altered areas are mineral concentrations of Mo, Cu, Sn, W, U, and F. Potassium feldspar samples from pegmatites, mineralized fracture zones, and mineralized greisen boulders were collected from three separate mineral occurrences of the New Ross area within the SMB. K-feldspar present in pegmatite samples from Long Lake and Walker Moly deposits, greisen samples from Long Lake, and hydrothermally mineralized samples from Millet Brook were used in this $^{40}Ar/^{39}Ar$ study.

The purpose of this study is to investigate the low-temperature thermal history at each of the three mineral occurrences by radiometrically dating the mineralized K-feldspar. It is hoped that the SMB age of 372 Ma is recorded within the feldspars and that this age will be isolated. The $^{40}Ar/^{39}Ar$ laser-probe method is used for this and the collected data are compared to existing data obtained from the incremental heating analysis of K-feldspar from the same samples. Aspects of the laser-probe method with respect to the accuracy of obtained mineral age estimates and the determination of spatial variation are favored over the incremental heating method. The laser-probe method for this study requires the fragmentation of feldspar crystals and analysis of the argon gas liberated from selected small fragments. This has the advantage of observing variations in the distribution of radiogenic argon within the feldspar grain and, hence, the age variations. For instance, it is common to find lower apparent ages calculated from rim fragments of minerals due to argon loss and higher apparent ages calculated from core fragments. However, step-heating analysis where argon gas is liberated from a mineral sample and analyzed at progressively higher temperature "steps" also has advantages. The data are graphically represented in a spectrum that can be used as an interpretive tool to understand samples that have suffered argon loss.

The K-feldspar ages are of interest as they reflect the age of mineralization in the New Ross area and also shed light on the thermal conditions present after mineral deposition. Previously, in addition to the K-feldspar $^{40}Ar/^{39}Ar$ step-heating analysis, muscovite samples from Walker Moly and Long Lake were dated and provide information on the age of the mineral deposits. This

study compares the results of the laser-probe analysis with the step-heating analysis results where small variations in the spatial distribution of radiogenic argon are not resolved. Mineralogical characteristics of these K-feldspars observed in thin section are also important in the discussion of apparent age variations obtained from both $^{40}Ar/^{39}Ar$ analyses.

1.1 Organization of Thesis

The thesis is divided into five chapters. The first section lays out what is covered, the problem to be investigated, and the basic intent of the study. Geological setting is the topic of the second chapter where the location and basic properties of the SMB are outlined. Specifically, the areas of interest where sample collection was conducted within the SMB are described in terms of location and mineral deposits present. There is a total of three sites and four feldspar samples; one sample from Walker Moly (pegmatite), one from Millet Brook (mineralized fracture), and two from Long Lake (pegmatite and mineralized greisen). Also included is a brief mention of the mechanisms responsible for the mineral deposits, which is the larger study that this $^{40}Ar/^{39}Ar$ thesis supplements. The third chapter deals with the methods and analytical techniques involved in recovering the feldspar from the granite samples and preparing the samples for irradiation and laser-probe analysis. The basis of the $^{40}Ar/^{39}Ar$ dating technique is included here. The operation of the Nd-YAG laser that is used in this study is presented along with the techniques that were used to obtain the data. Also, issues concerning poor laser coupling with the feldspars and the characteristics of the absorption spectrum of K-feldspar are investigated here. The fourth chapter deals with the $^{40}Ar/^{39}Ar$ geochronology and petrography including the results of the laser-probe analysis and comparison of these new data to the previously obtained data from the step heating analysis. Next, an examination of thin sections made from the sample is included. The fifth and final chapter comprises a summary of the data obtained in this study along with data obtained from the step-heating work on the same samples. Each sample is discussed individually, drawing together the information obtained from the $^{40}Ar/^{39}Ar$ analyses and the thin section observations. Interpretations are made for each sample. The geological significance of the results, interpretations, and conclusions follow. Recommendations for future research comprise the final section of this thesis.

Chapter 2: Geological Setting

2.1 Introduction

The four K-feldspar samples used for this geochronology study come from three mineral occurrences within the SMB. Each of these locations is discussed in this chapter following general remarks concerning the geological and geotectonic setting of the SMB and surrounding country rock. The samples consist of two pegmatites from the Long Lake and Walker Moly deposits, a greisen from the Long Lake deposit, and uranium-irradiated minerals from the Millet Brook deposit. Following the discussion of each of these three locations is a section on the formation of the deposits within the SMB.

2.2 Geological and Geotectonic Setting

The Meguma Zone is the most outboard terrane in the Canadian Appalachians and covers an area of approximately 200,000 km^2 (Schenk 1995). The Appalachians resulted from the collision between the Gondwanan and Laurentian continents marking, the closure of the Late Proterozoic–Ordovician Iapetus Ocean (Windley 1984). The tectonically stable, eroded remnants of the Lower Paleozoic mountain belt is what remains of the Appalachians today.

The Meguma Zone is last accreted lithotectonic terrane of the Canadian Appalachians (Williams & Hatcher 1982). The boundary between the Meguma Zone and the Avalon Zone to the north is marked by the Cobequid-Chedabucto Fault. Two dominant lithological components comprise the Meguma Zone: (1) Cambrian-Ordovician Meguma Supergroup of metamorphosed sandstone and shale that was deposited as a deep-sea turbidite fan complex and underwent regional deformation and metamorphism related to the Devonian Acadian Orogeny (Schenk 1995); and (2) Late Devonian peraluminous granitoid plutons (Figure 1).

Near the end of the Acadian Orogeny, after accretion of the Meguma Zone, granitoid plutons and syn-plutonic mafic dykes intruded the crust (Clarke et al. 1997). As summarized by Clarke et al. (1997), the granite emplacement is dated at 372 Ma. The peraluminous plutons of the South Mountain Batholith can be subdivided into early (phase 1) plutons consisting of granodiorite and biotite monzogranite as well as more evolved (phase 2) plutons consisting of leucomonzogranite and leucogranite (MacDonald et al. 1992). The mineral occurrences to be discussed here occur in the Salmontail Lake Pluton (phase 1) or the New Ross Pluton (phase 2).

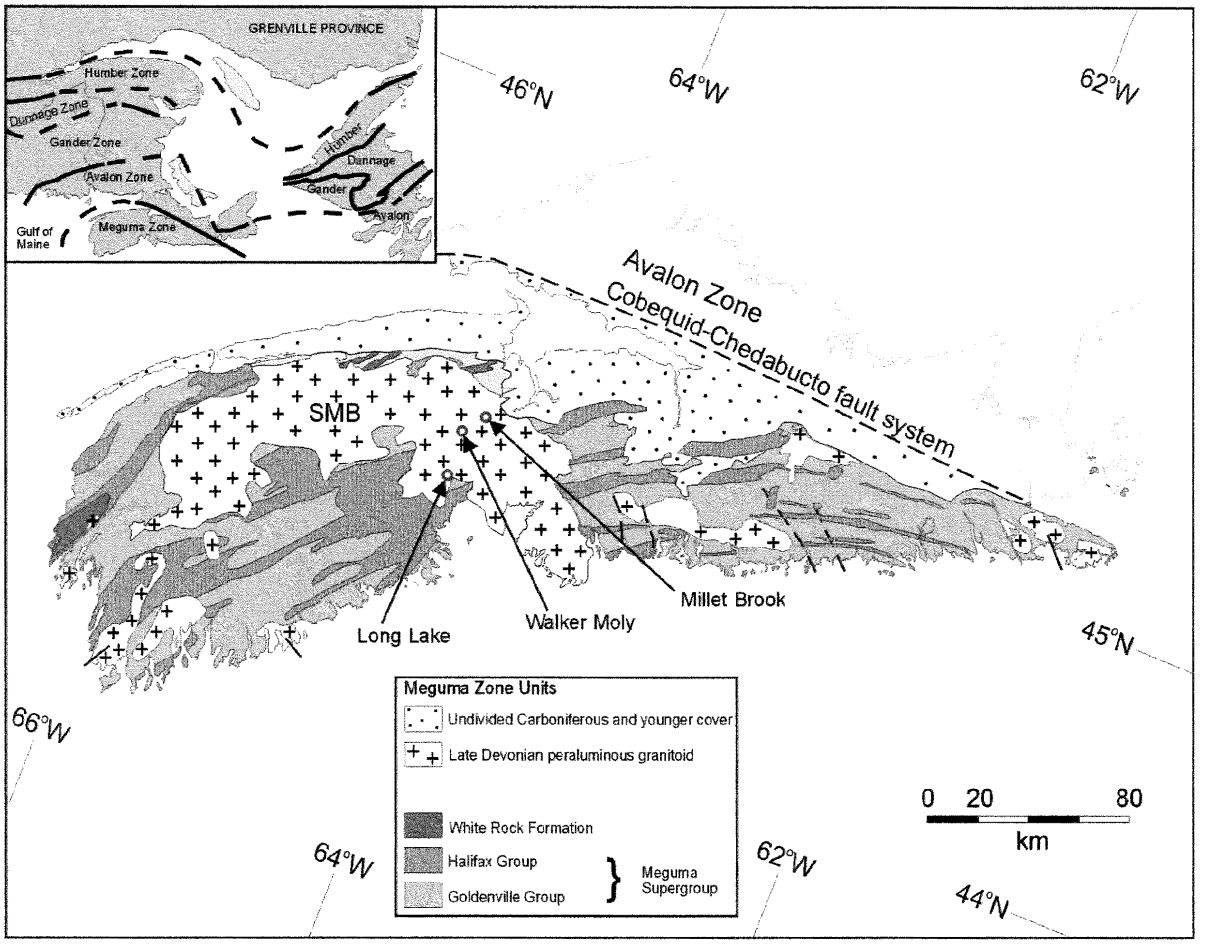

Figure 2.1: Geological Map of Nova Scotia showing the location of the New Ross area (courtesy of D. B. Clarke).

2.3 Mineral Deposits

The sample collection areas include the Long Lake area, the Walker Moly Prospect, and Millet Brook. Discussed here for each area are the host granitoid and pluton type, the location and accessibility of each area, deposit types, and mineral associations. The most of the following information, mainly the mineral associations for each area, are taken from MacDonald (in press) unless noted otherwise.

2.3.1 Long Lake Deposit

Leucogranite of the phase 2, New Ross Pluton hosts the Long Lake deposit. The deposit is located near the north end of Long Lake, Lunenburg County, to the east of Gold River and is accessible from the east and the west by woods roads, private logging roads, and woods trails. This area marks a shallow-dipping contact between the leucogranite of the South Mountain Batholith and the metamorphosed quartzites and greywackes of the Goldenville Group (O'Reilly

et al. 1982). Along this granite metasediment contact are greisen zones that can be traced for 230 m and range from 50-100 m in width. The term "greisen" is used here to indicate altered granite that is quartz- and muscovite-rich with fluids from the differentiation of the granite magma being responsible for this alteration. The alteration of the granite grades from microclinized granite to greisenized granite to greisen. This is marked by the alteration of potassic feldspar to quartz and muscovite (O'Reilly et al. 1982). Locally, greisen-type deposits occur as infillings along irregular fractures and also form as pods that are roughly circular in shape (O'Reilly et al. 1982). Well-developed greisen areas contains molybdenite, wolframite, fluorite, and copper sulphides. Samples of pegmatite at the Long Lake prospect were collected from rock dump boulders left over from previous work since the area is heavily overgrown and no outcrops of pegmatite were discovered. The boulders were located west of the greisen zone and consist of pegmatite and banded aplite deposits that are both predominantly associated with molybdenite.

2.3.2 Walker Moly Deposit

The mineral occurrences at the Walker Moly prospect are hosted by the phase 2, New Ross Pluton consisting of coarse-grained leucomonzogranite. This area is located around New Russel and is accessed by a woods trail 120 m south of the Windsor road at New Russel. Massive orthoclase pegmatite deposits with quartz, muscovite, and molybdenite intergrowths were collected here. The site consists of a dump and a sealed shaft, therefore samples were only obtained from the dump. Based on drilling conducted during an active period of exploration, the pegmatite was determined to form a northeast plunging dyke and is associated with medium-grained aplite (O'Reilly et al. 1982). Also spread along the dyke are sections of greisenized granite. Pegmatite, aplite, and greisen-associated mineralization are present in the rock dump samples. The minerals associated with both pegmatite and aplite are molybdenite and copper sulphides, the former being the mineral of primary interest during active exploration at this site. Associated with the greisen are molybdenite, wolframite, cassiterite, bornite, and chalcopyrite (O'Reilly et al. 1982).

2.3.3 Millet Brook Deposit

The Millet Brook deposit is hosted by the phase 1 Salmontail Lake Pluton of monzogranite and biotite granodiorite (Chatterjee & Strong 1984). The monzogranite hosting this deposit is white to gray in colour, biotite rich, and muscovite poor (O'Reilly 1992). It is situated about 50 km west-northwest of Halifax and is approximately 2.5 km north-northwest of a roof pendant of Goldenville Group metasedimentary rocks. This metasedimentary inlier forms the boundary

between the Salmontail Lake Pluton and the New Ross Pluton. The mineral deposits in this area occur as closely spaced en-echelon pods and lenses that are present within a fracture zone with a north easterly trend (Chatterjee & Strong 1984). Extending over a 240 m strike distance, the deposit contains an estimated 1.0 million pounds of U_3O_8 with an average grade of 0.15-0.20% U_3O_8 and is presently subject to an environmental moratorium (Chatterjee & Strong 1983; Carruzzo et al. in prep.). Because no outcrop is presently accessible at the site, the samples from Millet Brook used in this study come from drill cores. The dominant minerals associated with the Millet Brook deposit are uranium bearing minerals: pitchblende, autunite, torbernite; copper minerals: chalcopyrite, bornite, covellite, chalcocite; as well as galena, sphalerite, and wolframite (Chatterjee & Strong 1984). Alteration of the mineralized fractures in this area is primarily the result of a cupola and several late-stage dykes of leucomonzogranite that underlie the phase 1 Salmontail Lake Pluton (Chatterjee & Strong 1984).

2.4 Formation of Mineral Deposits

The main focus of Carruzzo et al. (in prep.) is a fluid inclusion study to understand the mechanisms and conditions of fluid circulation responsible for the formation of the mineral deposits at these three locations, as well as several other locations, within the New Ross area of the SMB. For instance, the Millet Brook deposit occurs in the Salmontail Lake Pluton but fluids produced by the more evolved intrusions beneath it have affected the types of mineral deposits that are present there. The relationship between the magmatic, metamorphic, and meteoric fluids and how they influence the types of mineral occurrences at each location is beyond the scope of this paper. However, the study of Carruzzo et al. (in prep.) yields $^{40}Ar/^{39}Ar$ muscovite ages from the Long Lake and Walker Moly mineral deposits as well as Re-Os dates for the molybdenite at Walker Moly. The analyses of muscovite and molybdenite suggest that these are primary mineral deposits formed during the emplacement of the SMB. This is a significant factor in the interpretation of ages obtained from the K-feldspar samples in this study.

Chapter 3: Methods and Analytical Techniques

3.1 Introduction

This section outlines the methods and analytical techniques that are involved in this laser-probe study of the New Ross area K-feldspars. Comprising this chapter is a discussion of sample selection in the field as well as mineral selection in the laboratory, the process of recovering the K-feldspar from the whole rock samples, and preparation of the samples for $^{40}Ar/^{39}Ar$ dating. Rims of the feldspar crystals were separated from cores in three of the four samples. A rundown of the apparatus that is used in the study, including the Nd-YAG laser, and the methods that were employed are covered here. Brief information on the methods and analytical techniques from the previous thermochronology study is also outlined.

3.2 The Basis of $^{40}Ar/^{39}Ar$ Dating

The following is summarized from Dickin (1995) and Attendorn & Bowen (1997). The $^{40}Ar/^{39}Ar$ dating method is based on the radioactive decay of ^{40}K to the stable daughter isotope ^{40}Ar. The assumption is made that no amount of ^{40}Ar initially exists in the mineral. This is the basis of K-Ar dating from which the $^{40}Ar/^{39}Ar$ method has evolved. With the $^{40}Ar/^{39}Ar$ method, a sample is irradiated in a nuclear reactor where it is bombarded with fast neutrons that convert ^{39}K to ^{39}Ar by neutron capture and proton emission. A flux monitor is also irradiated with the sample to determine the proportion of ^{39}K that has been converted to ^{39}Ar. From the well-known age of the flux monitor, an irradiation parameter (J) can be calculated. The proportion of $^{40}Ar/^{39}Ar$ can now be calculated for the sample. ^{40}Ar is the radiogenic argon produced by the radioactive decay ^{40}K. Because the proportion of $^{39}K/^{40}K$ is constant in nature and the amount of ^{39}K is known through the measurement of ^{39}Ar after irradiation, the apparent age can be calculated from the $^{40}Ar/^{39}Ar$ ratio as follows:

$$t = 1/\lambda \ln [1 + J (^{40}Ar/^{39}Ar)]$$

$t \equiv$ apparent age, $\lambda \equiv$ decay constant, $J \equiv$ irradiation parameter (dimenstionless).

The flux monitor is of a known age in order to obtain a J-value:

$$J = [\exp(\lambda t) - 1] / (^{40}Ar/^{39}Ar)$$

$t \equiv$ age of the standard sample.

The benefit of $^{40}Ar/^{39}Ar$ over K-Ar dating is that the isotopic measurements can be made at the same time by the same method (mass spectrometry) thus introducing less error in the age calculation.

3.3 Sample Selection

The samples collected and used for the purpose of the $^{40}Ar/^{39}Ar$ analysis were visibly fresh and free of significant alterations or inclusions. A summary of the samples used in this study, including the sample number, location, and type is listed in Table 3.1. Some of the samples used in this study have been collected previously by Carruzzo et al (in prep) for age spectrum analysis. Carruzzo did not previously analyze Long Lake K-feldspar from mineralized greisen obtained from rock dump boulders. The other samples for this study collected during the same field outing (SC-12L and SC-9W) were from the same sites as those collected for previous studies. Essentially, newly collected samples (SW-LL01, SC-12L, SC-9W) as well as the previously collected samples (SC-12L, SC-9W) were used all in this $^{40}Ar/^{39}Ar$ study.

Sample Number	Location	Sample Type
SC-12L	Long Lake	Pegmatite
SW-LL01	Long Lake	Mineralized Greisen
SC-9W	Walker Moly	Pegmatite
DK-MB-99-01	Millet Brook	Mineralized Fracture

Table 3.1: Samples used in this study along with the respective locations of occurrence and the type of sample.

Care was taken when selecting feldspar from Long Lake mineralized greisen as most of the K-feldspar was on the surface. The greisen boulder was sufficiently broken up as to yield pieces of feldspar from within the rock. Selecting feldspars on the surface of the rock for $^{40}Ar/^{39}Ar$ analysis may yield an inaccurate age where even relatively minor thermal or fluid events could partially reset the isotopic signature of the K-feldspar (Attendorn & Bowen 1997).

The K-feldspar from Millet Brook differs significantly from those samples collected from both Long Lake and Walker Moly. The K-feldspar is not syn-mineralization at Millet Brook, but just part of the rock that is altered during the mineralizing event. No samples were collected directly at Millet Brook on account of the environmental moratorium affecting the area. Drill core fragments were therefore used and were of a limited supply. Also, the feldspar grain sizes were much smaller in the Millet Brook sample than in the other samples. The sizes were on the order of millimeters whereas the other samples possessed feldspar grain sizes on the order of centimeters.

3.4 K-Feldspar Recovery

Physical methods were employed to extract the feldspar grains from the whole rock for samples SW-LL01, SC-12L, and SC-9W while K-feldspar separate from the samples from Millet Brook was already available from the study of Carruzzo. In general, the feldspars were removed from each sample using a hammer, cold chisel, and metal picks along with pliers to crush the rock surrounding the K-feldspar grains. Care was taken to remove the feldspar grains in a relatively intact state so that grain rims and cores could be later separated. Two or three grains were removed from each sample for analysis.

Sample SC-12L possessed well-defined feldspar grains surrounded mainly by quartz. The feldspar is a pale yellow colour and could easily be distinguished from the white quartz. A photograph of a cut piece of the pegmatite showing the white quartz and pale yellow and orange K-feldspar along with associated molybdenite is shown in Figure 3.1. Removal of the grains was relatively clean with the edges of the grains remaining intact after removal. Small inclusions of quartz, muscovite, and dark minerals were present within the outer 1-2 mm of the grain and even larger quartz inclusions (3-4 mm) were present within the feldspar. A sketch of a representative grain is displayed in Figure 3.2.

The recovered K-feldspar from the greisen sample SW-LL01 was more easily removed from the rock than in the previous sample and remained well intact. The easy removal is due to the slightly crumbly texture of the greisen and the distinct light colour of the feldspar. The colour of the feldspar is generally pale yellow with cloudy rust-coloured portions. There were very few inclusions present within the grains and consisting of quartz and muscovite. Fragments containing these visible small inclusions were not used in the laser-probe analysis. Figure 3.3 is a sketch of a representative grain. Photographs of the greisen sample in the field are shown in Figures 3.5a and 3.5b.

The K-feldspar from Sample SC-9W was not as discrete as in the other samples and was interspersed with quartz. Some grains, such as those similar to the ones in the sketch (Figure 3.4), were definable with sharp edges where they occurred next to quartz. The feldspar is generally light pink in colour. The grains from Sample SC-9W were more difficult to remove than in the other samples because the rock is harder and the K-feldspar occurs frequently with quartz.

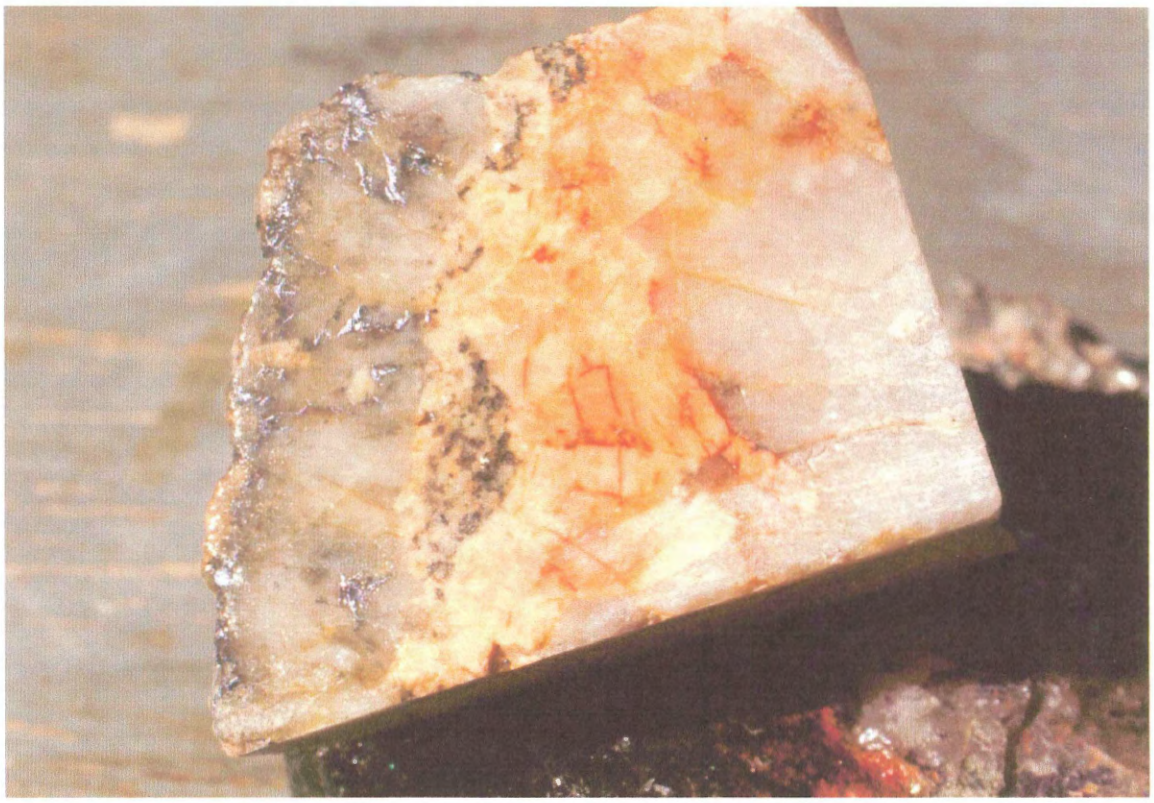

Figure 3.1: Photograph of pegmatite sample from Long Lake cut to show quartz (white), K-feldspar (yellow and orange), and associated metals.

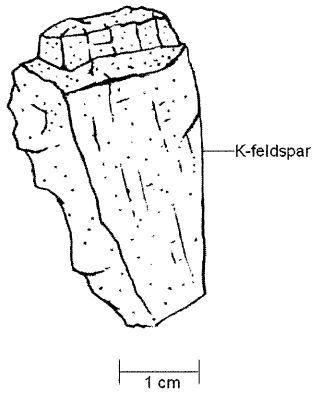

Figure 3.2: Representative sketch of K-feldspar from Sample SC-12L.

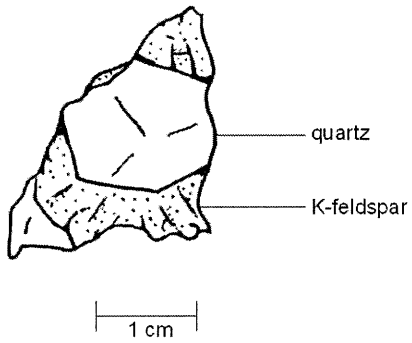

Figure 3.3: Representative sketch of K-feldspar from Sample SW-LL01.

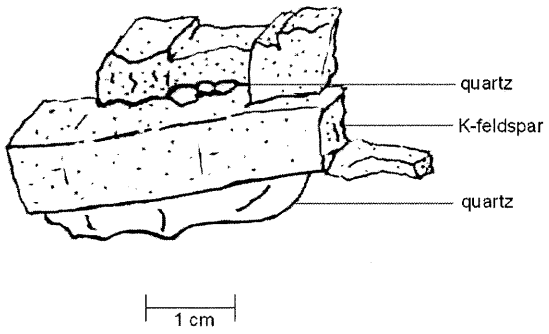

Figure 3.4: Representative sketch of K-feldspar from Sample SC-9W.

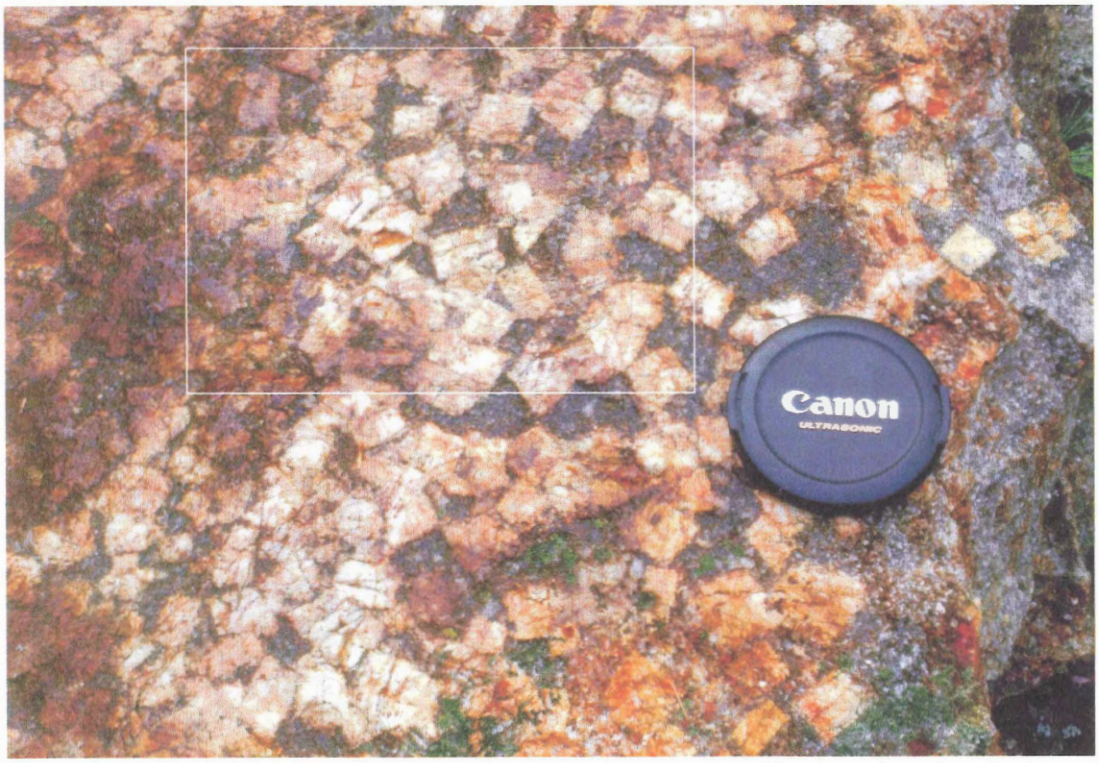

Figure 3.5a: Photograph of the greisen in the field at Long Lake. The light coloured laths of K-feldspar are 2-3 cm in size.

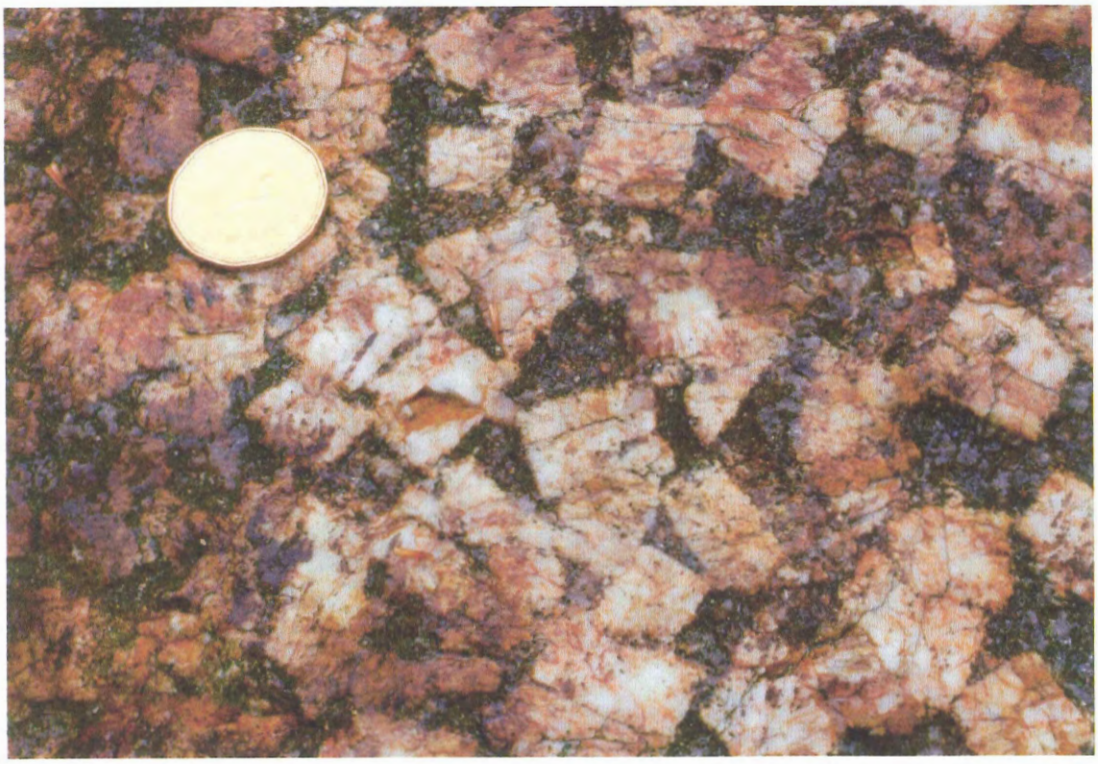

Figure 3.5b: Close-up image of outlined portion of Figure 3.4a. The rust-coloured alteration and the macroscopic texture of the laths are better displayed here. Dollar coin for scale.

3.5 Sample Preparation

Once the K-feldspars were removed from each sample they next had to be broken into sub-millimeter sized fragments. These small fragments produced from each of the feldspar samples are to be used in the laser-probe $^{40}Ar/^{39}Ar$ analysis. The rims of the feldspar crystals were separated from the cores in order to detect the possible variation in the measured $^{40}Ar/^{39}Ar$ ratio (i.e. there may be lower apparent ages determined for the rims and higher apparent ages for the cores). Successful separation of rims from cores depended on the difficulty of fragmentation of each of the feldspar samples and how well defined the actual edges of the crystals were. The rims of SC-12L are taken from the outer 1-2 mm of the feldspar crystals, the rims of SW-LL01 are defined to be within the outer 2-4 mm, and the rims of SC-9W are from the outer 2-3 mm. Rims were not separated from cores for sample DK-MB-99-01. The fragments were then closely checked to see that they did not contain any visible inclusions or other minerals from the host rock.

Selected fragments from each sample were then placed into 1-2 mm diameter pits that had been drilled in small (about 2 cm diameter) aluminum disks that served as mounts for around 20-30 fragments each. Figure 3.6 is a photograph of the disk containing feldspar fragments from sample SC-9W. These disks along with the hornblende standard MMHb-1 were shipped to McMaster University for irradiation. The MMHb-1 standard has a known age of 520.4 ± 1.7 Ma (Sampson & Alexander 1987).

3.6 Apparatus and Techniques

The instrumentation used in this study includes a Nd-YAG laser-probe, a modified petrographic microscope equipped with a video camera and display monitor, and a VG3600 mass spectrometer. A schematic the laser-probe facility at the Australian National University is shown in Figure 3.7 and is fundamentally identical to the layout at Dalhousie University. Some aspects of the extraction system depicted in this diagram are not quite similar to configuration used for this study.

This laser-probe study employs a Quantronix 117 Nd-YAG laser. It was operated in TEM_{00} mode with a 17-Watt output. The TEM_{00} mode yields the minimum focused laser spot diameter which is typically 10-20 times the wavelength of the radiation. A beam with a Gaussian power distribution is produced in this mode (McDougall & Harrison 1999). The wavelength of the Nd-YAG laserprobe is 1064 nm. Favorable aspects of a laser-probe for the purposes of

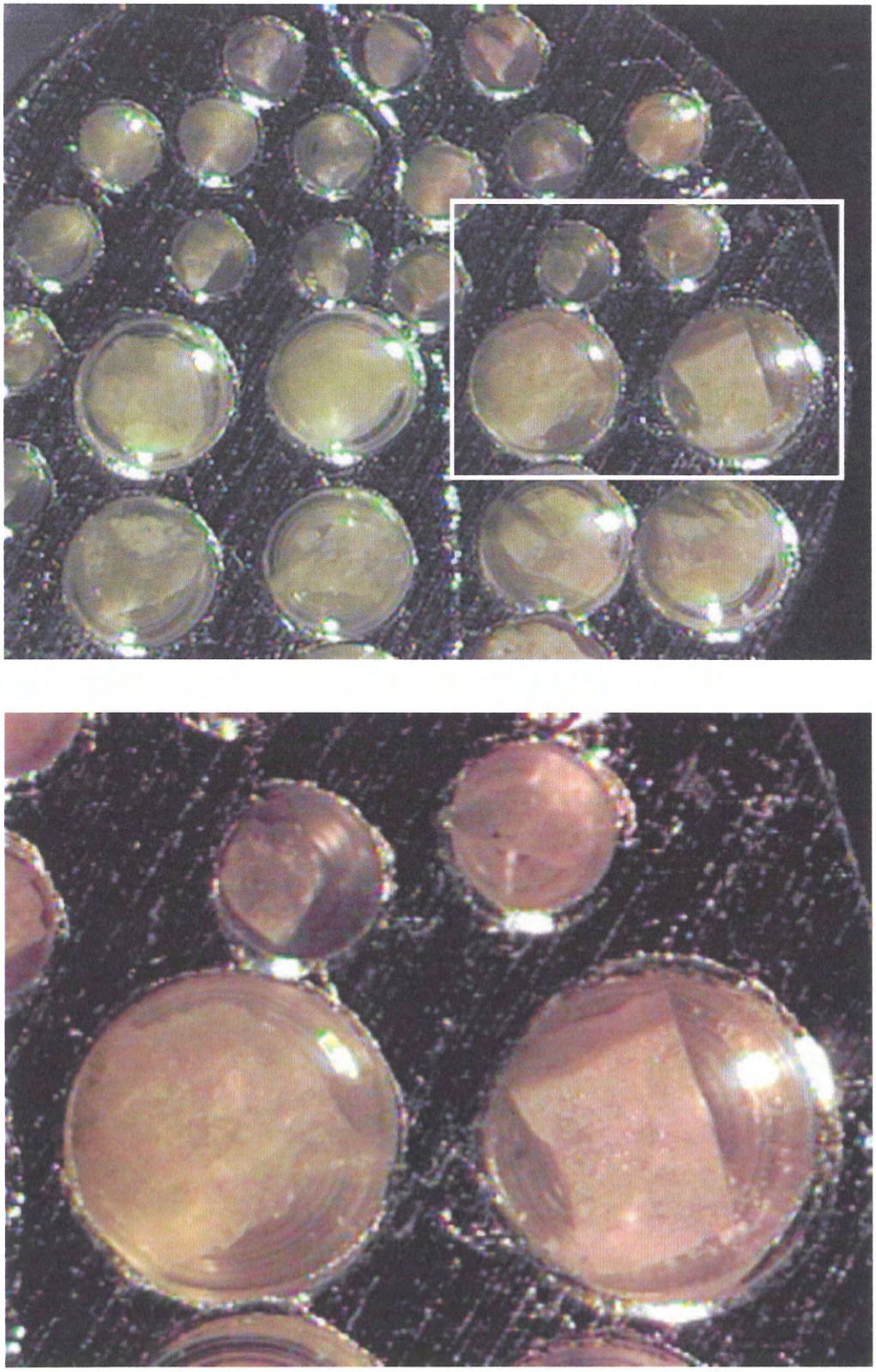

Figure 3.6: Photograph of the drilled aluminum disk. The sample fragments contained here are SC-9W fragments from Walker Moly. The larger machined holes are 2 mm in diameter and the smaller holes are 1 mm in diameter.

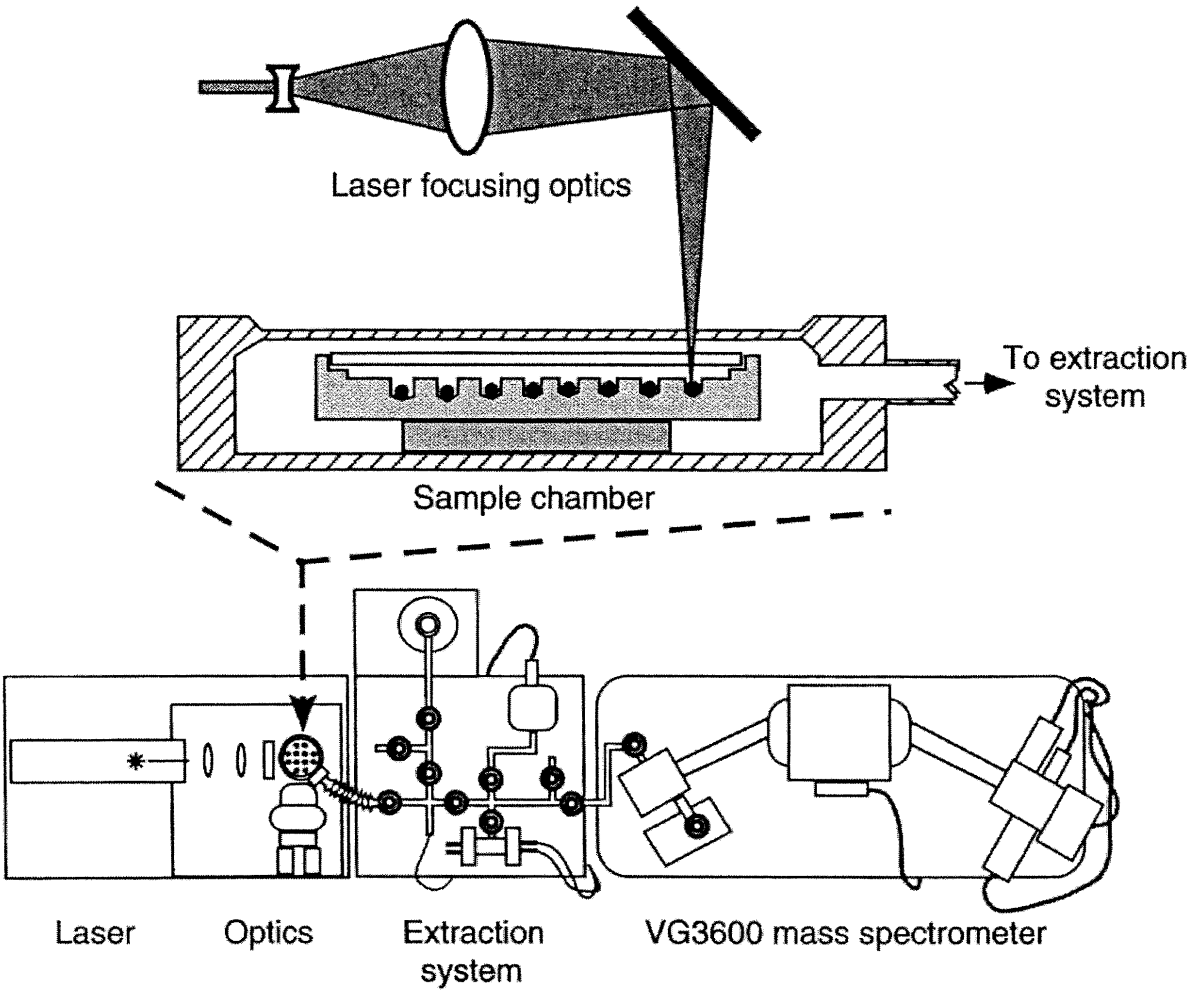

Figure 3.7: Schematic overhead view of the overall layout of the laser-probe facilities at ANU showing detail of the laser focusing on a crystal in the sample chamber. This layout is quite similar to the layout at Dalhousie University (from McDougall & Harrison 1999; Figure 3-13).

$^{40}Ar/^{39}Ar$ dating are small beam divergence and suitable wavelength (taking into account the absorbance characteristics of the mineral to be analyzed). Optimum conditions result in a beam with an adequate power density or focused spot size (measured in Watts per meter, Wm^{-2}). Small beam divergences, on the order of less than 10 mrad, allow for high energy intensities and efficient collection and focusing (McDougall & Harrison 1999). The relevance of wavelength suitability is illustrated in Figure 3.8 as well as in Table 3.2. Laser spot size is not an important factor in this study because the laser is used here to heat the entire feldspar fragment, not just a discrete portion of it.

The fragments of K-feldspar were completely out-gassed using laser heating. A calcite attenuator in the beam delivery device regulates the laser beam intensity and thus controls the amount of energy that is incident upon a sample. In practice, a sample is moved under the laser beam using the x-y translation stages until the entire fragment is adequately heated. The Nd-YAG is typically not recommended for dating alkali feldspars on account of problems encountered with beam coupling (McDougall & Harrison 1999). This means the feldspar cannot be sufficiently heated by the laser. Whether the laser beam couples well with a mineral depends on the structure and opacity of the mineral and the wavelength of the laser. Minor instances of poor beam-feldspar coupling were observed, as outlined in the next chapter. As noted by McDougall & Harrison (1999), workers have overcome severe problems of laser coupling by including a fragment of dark basaltic glass that has been completely degassed. The dark glass absorbs the radiation and aids in the melting of the mineral grain. For this study, the use of a small amount of carbon on the surface of the feldspar fragment was considered in order to couple the beam effectively; however, this proved to be unnecessary. Another potentially viable solution would be to wrap the sample in gold leaf.

Once the small amount of gas is released from the sample it is expanded into an ultrahigh vacuum (UHV) system. Purification of the gas takes place in this system before it is emitted to the mass spectrometer for isotopic analysis. The entire extraction system is metal and has been pre-baked in order to obtain the lowest possible argon blanks (i.e. background argon readings in the absence of a sample). Corrections applied on the raw isotopic data include discrimination corrections for the mass spectrometer, corrections for interfering isotopes (i.e. argon isotopes produced in the nuclear reactor other than ^{39}Ar, the isotope used here), corrections for system blanks, and finally, one to correct for the presence of any small amount of atmospheric argon in the sample.

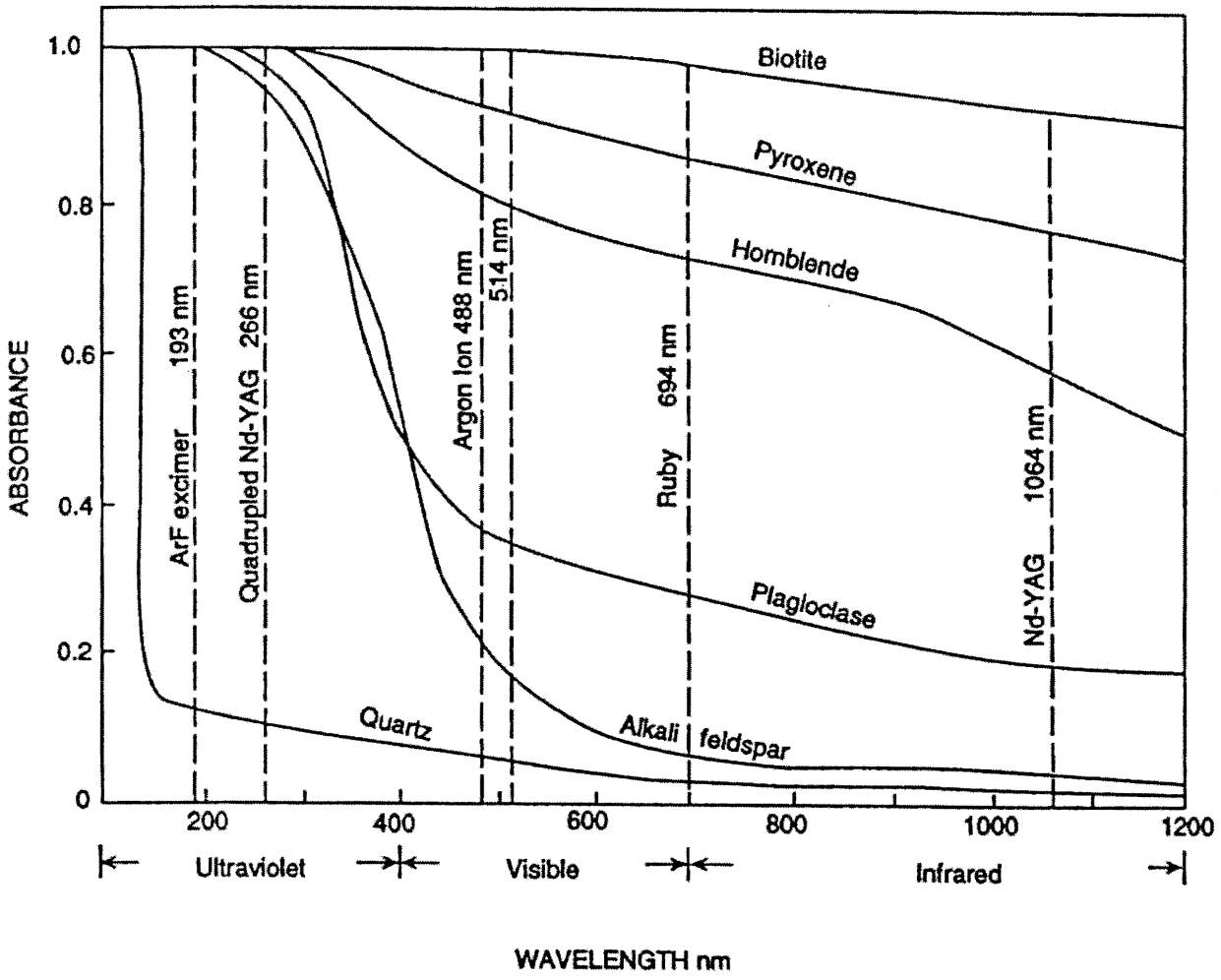

Figure 3.8: Absorption spectra for a number of silicates including alkali feldspar. Note the very low absorbance of alkali feldspar at the Nd-YAG wavelength of 1064 nm (as cited in McDougall and Harrison, 1999; Figure 3-19).

Laser Type	λ (nm)	Typical output energy	Typical repetition rate (Hz)	Typical pulse length (μs)	Minimum diameter spot size (μs)
Pulsed					
Nd-YAG	1064	~ 0.25 J/pulse	10	250	~ 20
Nd-glass	1054	~ 0.35 J/pulse	0.1	200	~ 25
Ruby	694	~ 0.2 J/pulse	0.02	150	~ 10
ND-YAG (frequency quadrupled)	266	≤ 0.02 J/pulse	10	0.01[a]	< 10
ArF excimer	193	~ 0.2 J/pulse	10+	0.02	≪ 10
Continuous Wave					
CO_2	10, 600	0-10 W+	-	-	~ 100
Nd-YAG	1064	0-20 W+	-	-	~ 20
Argon ion	Mainly 488 and 514	0-20 W+	-	-	~ 10

[a] Q-switched, λ ≡ wavelength

Table 3.2: Characteristics of lasers used in $^{40}Ar/^{39}Ar$ dating applications. The Nd-YAG laser used at Dalhousie University can be operated in both pulsed and continuous wave modes (modified from McDougall & Harrison, 1999; Table 3-6)

The step-heating $^{40}Ar/^{39}Ar$ analysis of feldspar from samples SC-9W, SC-12L, and DK-MB-99-01 was conducted previously by Carruzzo et al. (in prep). The samples were heated incrementally and the $^{40}Ar/^{39}Ar$ ratio, and hence apparent age, determined for each successive temperature step. The data are displayed graphically with the age (Ma) on the vertical axis, which is proportional to the $^{40}Ar/^{39}Ar$ ratio, and the percentage of ^{39}Ar released, ranging from 0% at the lowest temperatures to 100% at the highest temperatures, on the horizontal axis. The total gas age is a weighted-average of the argon ratios calculated at each successive temperature step. Therefore, the apparent ages determined for the low percentage release of ^{39}Ar have a lesser impact on the total gas age. The advantage with the step-heating method is that progressive outgassing makes it possible to identify and exclude anomalous sub-systems within the sample in order to date the "properly behaved" parts in the spectrum (Dickin 1995).

A general comment about the interpretation of $^{40}Ar/^{39}Ar$ data obtained from both methods is best stated before discussing the results. In an ideal closed system, an idealized feldspar crystal will not have been reheated or otherwise thermally disturbed after rapid cooling below the temperature at which radiogenic argon is retained within the mineral, known as the closure temperature. In such a case, the laser-probe analysis would yield a constant $^{39}Ar/^{40}Ar$ ratio for

each fragment of the feldspar sample. In addition, the step heating analysis would yield a flat age spectrum indicating a constant $^{40}Ar/^{39}Ar$ ratio calculated at each progressive temperature step. However, minerals experience argon loss through heating events and argon loss by the natural process of diffusion. At low temperatures in the step heating analysis of partially disturbed feldspar, the domains most susceptible to argon loss through diffusion will be outgassed producing anomalies in the spectrum. At higher temperatures, the argon bound in the lattice of the feldspar should be released (Dickin 1995). In this case, a relatively concordant portion of the spectrum, or sometimes what is known as a "plateau", may occur in the age spectrum. These may better reflect the actual crystallization age of the feldspar (Attendorn & Bowen 1997). Lee et al. (1991) identified criteria for the characterization of a plateau. A set of adjacent steps, each of which must yield an age within two standard deviations (2σ) of the mean age, has to contribute more that 50% of the total argon release in order to be considered a plateau.

Presently, the step-heating analysis of K-feldspars is of great interest to the study of argon diffusion. The anhydrous nature of feldspars makes them very suitable for diffusion studies in the vacuum extraction furnace (Harrison 1990). The process of argon diffusion and the interpretation of age spectrum data are topics of debate for many researchers (Parsons et al. 1999; Wartho et al. 1999; McDougall & Harrison 1999) and are beyond the scope of this study.

Chapter 4: $^{40}Ar/^{39}Ar$ Geochronology and Petrography

4.1 Introduction

This section includes the $^{40}Ar/^{39}Ar$ results and observations from the present laser microprobe dating study and the results obtained from the previously conducted conventional step-heating $^{40}Ar/^{39}Ar$ analysis of K-feldspar from the same sample areas. A general rundown of features observed in a thin section from each sample is also included in this chapter.

4.2 Results of Laser Microprobe Analysis

This section is devoted to the results that were obtained from the laser microprobe liberation of Ar gas from the samples and also the behavior of the grains as they were heated with the laser. After the $^{40}Ar/^{39}Ar$ ratio is measured for each fragment and the appropriate corrections made, an apparent age can be calculated using the appropriate J-value from analysis of the MMHb-1 flux monitor.

When the laser was initially activated at low power, none of the fragments showed any obvious signs of heating or swelling. As the energy was increased using the calcite attenuator, the effects of this heating could be observed on the video monitor. The portions of the fragment directly under the laser first bulged and released small amounts of melt. As the heat increased, this area glowed as it melted and resembled a bubbling viscous fluid. After several seconds of heating the same area, the bubbling action ceased. The stage was then moved with the laser still incident on the grain fragment in order to melt the entire sample. After thoroughly subjecting the whole fragment to the laser beam, the operator would note no more noticeable bubbling or physical effect and the grain was thus considered to be completely degassed. What remained of the fragment after heating was a glassy, amorphous bead.

All four of the samples behaved very much the same way under the laser. There was, however, some notably poor coupling with the Millet Brook feldspar fragments, DK-MB-99-01. The laser energy had to be stepped up more than with the other samples in order to produce the same physical effects of melting. This was the only instance of poor coupling noted in this study.

The feldspar fragments from each sample are analyzed and plotted on a graph with the apparent age in millions of years on the vertical axis and the measured amount of ^{39}Ar released on the

horizontal axis. The amount of ^{39}Ar is proportional to the size of the fragment and is measured in mV, an arbitrary unit obtained directly from the mass spectrometry analysis. Red bars indicate the data from the pieces defined as rim fragments while black bars indicate the core fragment data. The horizontal error bars on each plot are entirely associated with the mass spectrometer measurement of ^{39}Ar. This instrument uncertainty is systematic and depends on the measured quantity of ^{39}Ar (2σ level of uncertainty). The vertical error bars also include the mass spectrometer uncertainty. In addition, the uncertainties with the other corrections that are stated in Section 3.6 are included in the apparent age error bars. Figures 4.1 to 4.4 are the apparent age plots for each sample. The data sheets from each analysis are included in Appendix 1.

Six feldspar fragments were selected for analysis from Long Lake mineralized greisen sample SW-LL01 with one fragment that had been defined as being from the rim of the feldspar (Figure 4.1). The mean age, calculated from the $^{40}Ar/^{39}Ar$ ratio, is 260.4 ± 2.8 Ma (Appendix 1). The age uncertainty includes the error in the irradiation parameter J (0.002533 ± 0.000025). The rim yields an age of 265.0 ± 4.1 Ma. The apparent ages of the cores range from 258.7 ± 4.0 to 265.3 ± 3.9 Ma with a mean value of 260.4 ± 3.2 Ma.

For the Long Lake pegmatite sample SC-12L, twenty-five fragments were analyzed, with thirteen rim and twelve core fragments. The calculated mean age is 319.6 ± 3.0 Ma for the obtained J-value of 0.002496 ± 0.000025 (Figure 4.2, Appendix 1). There is significantly more scatter in these results than in SC-9W. The range of apparent age calculations for the rims is from 305.2 ± 4.3 to 344.5 ± 5.3 Ma with a mean of 327.1 ± 8.3 Ma. The range of apparent age calculations for the cores is from 279.5 ± 4.7 to 353.0 ± 6.3 Ma with a mean of 323.4 ± 20.9 Ma.

Twenty-four fragments of the Walker Moly pegmatite sample SC-9W were analyzed with thirteen rims and eleven cores. A mean age of 342.9 ± 3.2 Ma was obtained for a J-value of 0.002514 ± 0.00025 (Figure 4.3, Appendix 1). From Figure 4.2, the apparent ages of the fragments appear to be closely clustered. The apparent ages of the rims range from 335.4 ± 5.2 to 351.9 ± 5.7 Ma with a mean value of 346.2 ± 4.0 Ma. The apparent of the cores range from 336.2 ± 4.8 to 347.1 ± 5.0 Ma with a mean value of 342.7 ± 2.7 Ma.

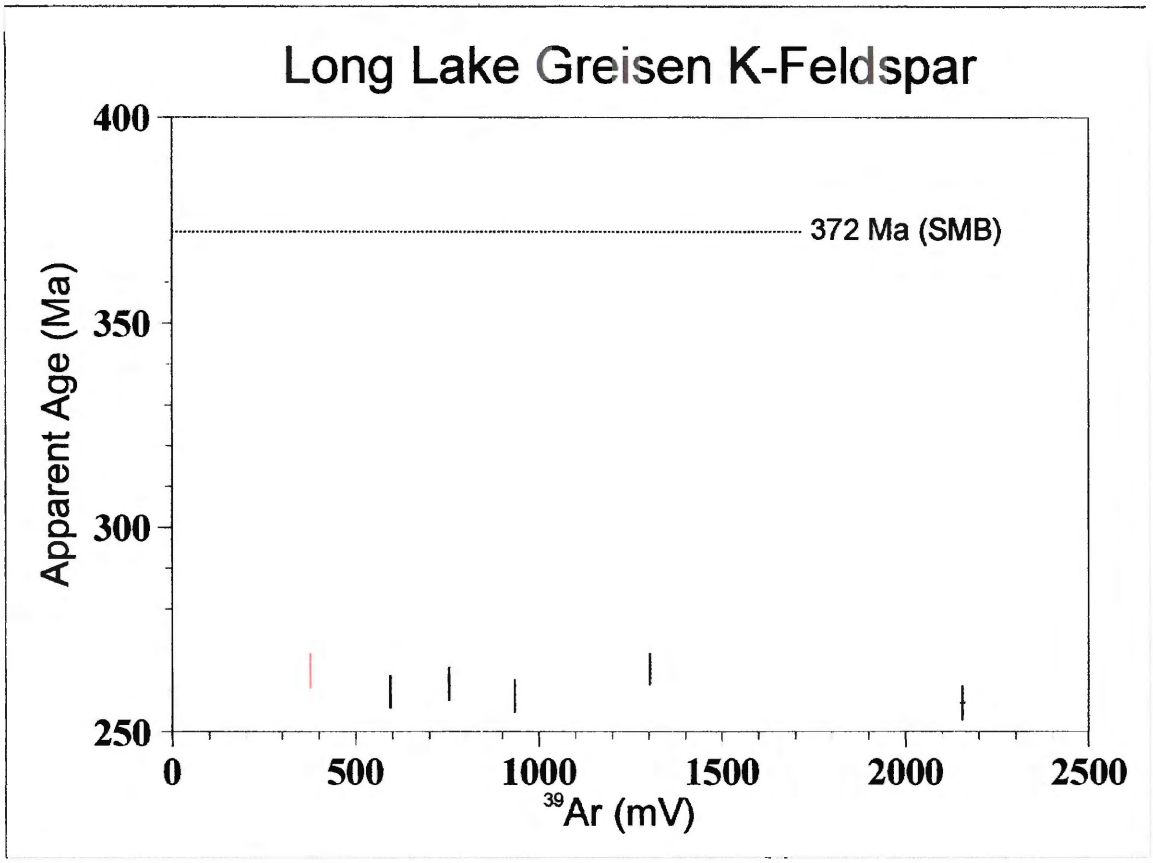

Figure 4.1: Results of the laser-probe $^{40}Ar/^{39}Ar$ analysis of SW-LL01. The red bar represents rim fragments whereas the black bars indicate fragments from the core. Six fragments were analyzed in total yielding a mean age of 260.4 ± 2.8 Ma.

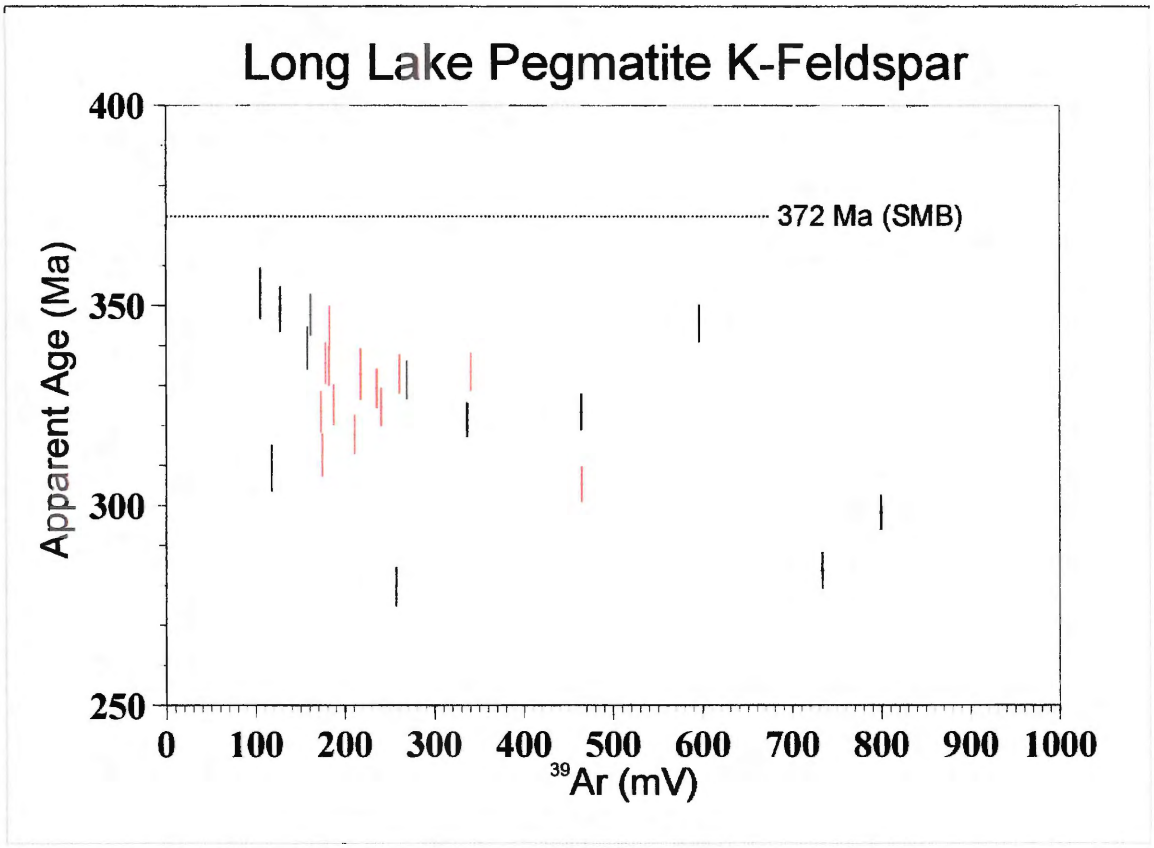

Figure 4.2: Results of the laser-probe $^{40}Ar/^{39}Ar$ analysis of SC-12L. The red bars represent rim fragments whereas the black bars indicate fragments from the core. Twenty-five fragments were analyzed in total yielding a mean age of 319.6 ± 3.0 Ma.

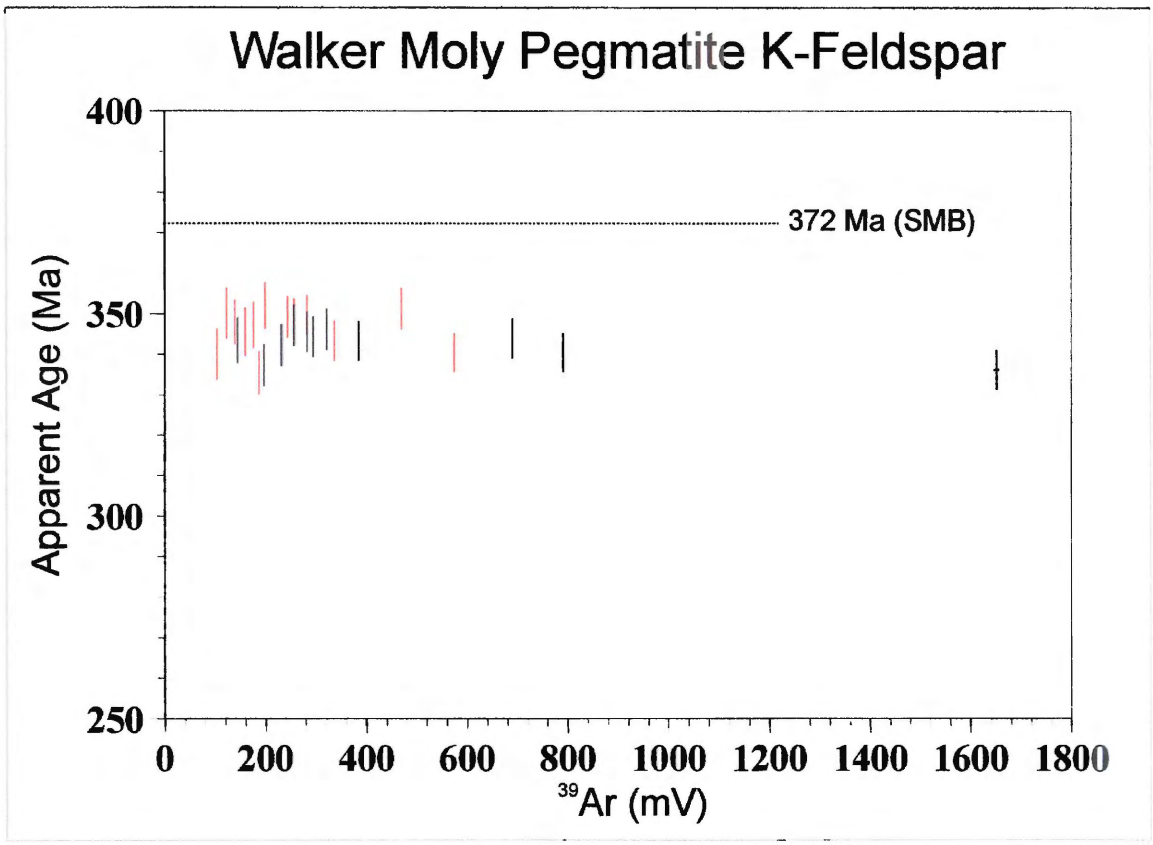

Figure 4.3: Results of the laser-probe $^{40}Ar/^{39}Ar$ analysis of SC-9W. The red bars represent rim fragments whereas the black bars indicate fragments from the core. Twenty-four fragments were analyzed in total yielding a mean age of 342.9 ± 3.2 Ma.

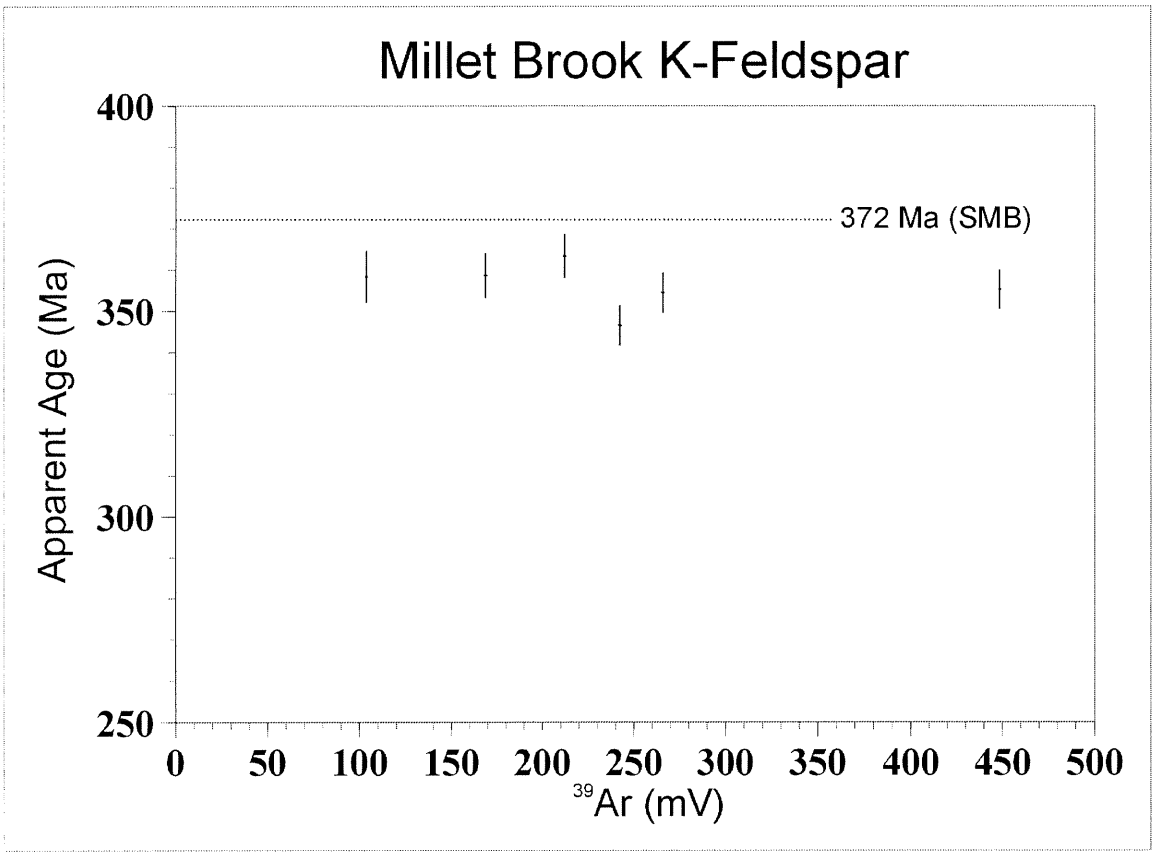

Figure 4.4: Results of the laser-probe $^{40}Ar/^{39}Ar$ analysis of DK-MB-99-01. There was no distinction made between rims and cores. Six fragments were analyzed in total yielding a mean age of 355.4 ± 3.5 Ma.

Six fragments of the Millet Brook mineralized fracture sample DK-MB-99-01 were analyzed. This is the sample that was prepared from pre-existing bulk separate so the rims and cores cannot be identified. The apparent age calculations range from 346.5 ± 4.8 to 363.4 ± 5.3 Ma with a mean age for this sample of 355.4 ± 3.5 Ma. The J value is 0.002552 ± 0.00025 (Figure 4.4, Appendix 1.4).

4.3 Results of Conventional Step-Heating Analysis

Previous work on the K-feldspar separates from the same locations yielded conventional step-heating $^{40}Ar/^{39}Ar$ age spectra. Sample SW-LL01 was not previously analyzed so there are no step-heating data available.

The pegmatite sample SC-12L from Long Lake was heated over a temperature range from 550 to 1450 °C. The total gas age, determined from the resulting age spectrum, is 327.0 ± 2.1 Ma (Figure 4.5, Appendix 2). The most noticeable feature of this age spectrum is the significant degree of discordance across the spectrum. Ages decrease to a minimum at around 30% ^{39}Ar release, followed by a progressive increase at higher temperature steps. The spectrum for this sample is much more discordant than the one for sample SC-9W. The portion of the spectrum from 30.8 to 99.2% ^{39}Ar release (temperature steps 940 to 1250 °C) ranges in age from 310.6 ± 5.2 to 346.3 ± 6.4 Ma.

The pegmatite sample SC-9W from Walker Moly was heated over a temperature range from 550 to 1500 °C. The total gas age, determined from the resulting age spectrum, is 347.9 ± 2.3 Ma (Figure 4.6, Appendix 2). The age spectrum here is relatively flat from around 30% ^{39}Ar release onwards with a slight age increase at successively higher temperatures. The lower part of the spectrum shows a small hump at around 12% ^{39}Ar. Excluding the low temperature argon release and considering the relatively concordant portion of the spectrum from 26.8 to 98.7% ^{39}Ar release (temperature steps 940 to 1250 °C) yields an age range from 342.4 ± 2.4 to 358.6 ± 3.4 Ma.

The mineralized fracture sample DK-MB-99-01 from Millet Brook was also heated over a temperature range from 550 to 1450 °C. The total gas age obtained from the age spectrum is 358.5 ± 2.2 Ma (Figure 4.7, Appendix 2). The spectrum is noticeably flat from around 30% ^{39}Ar release onward with a slight progressive increase in age with increasing temperature. The apparent ages from the spectrum from 0-15% appear to slightly increase and then drop again from

15-20%. The age range of the spectrum from 20.5 to 96.4% ^{39}Ar release (temperature steps 1000 to 1250 °C) is from 353.5 ± 2.1 to 360.4 ± 1.9 Ma.

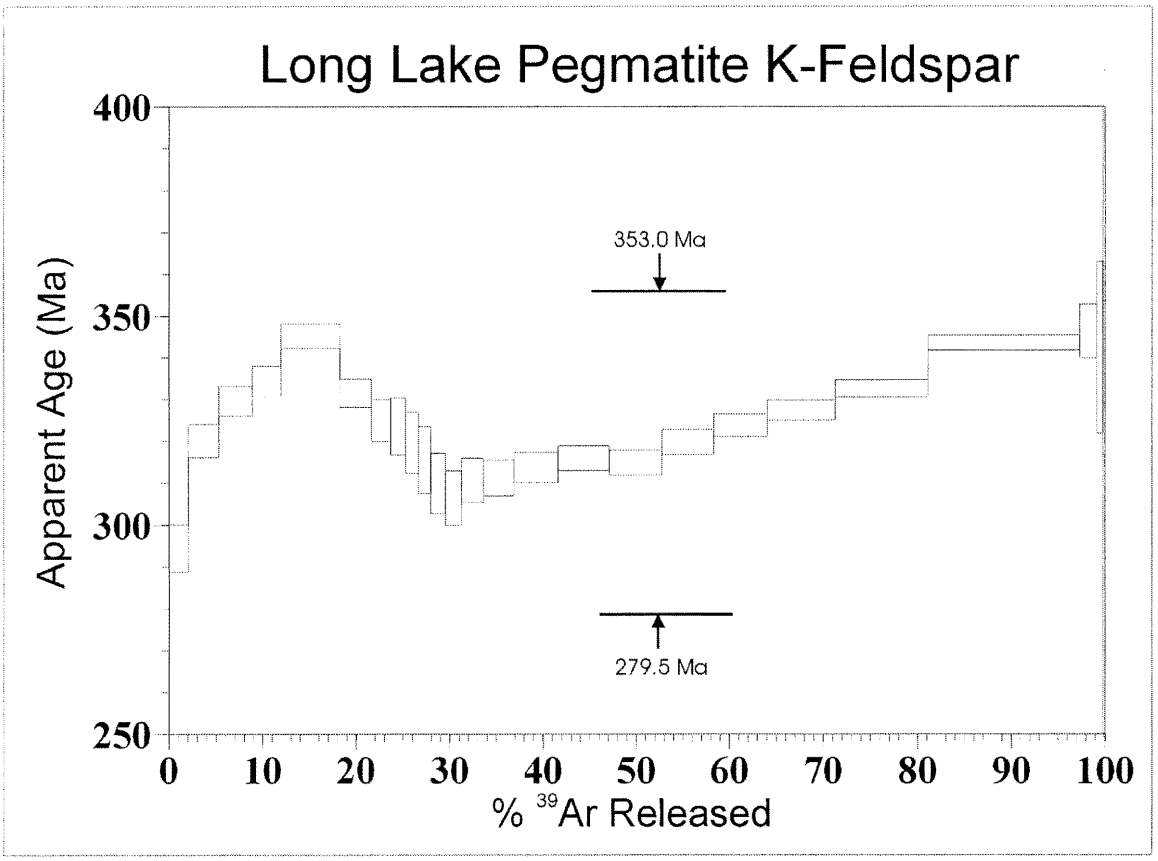

Figure 4.5: Conventional step-heating $^{40}Ar/^{39}Ar$ analysis of SC-12L from previous work. The laser-probe age range is displayed on the spectrum. The total gas age for this sample is 327.0 ± 2.1 Ma.

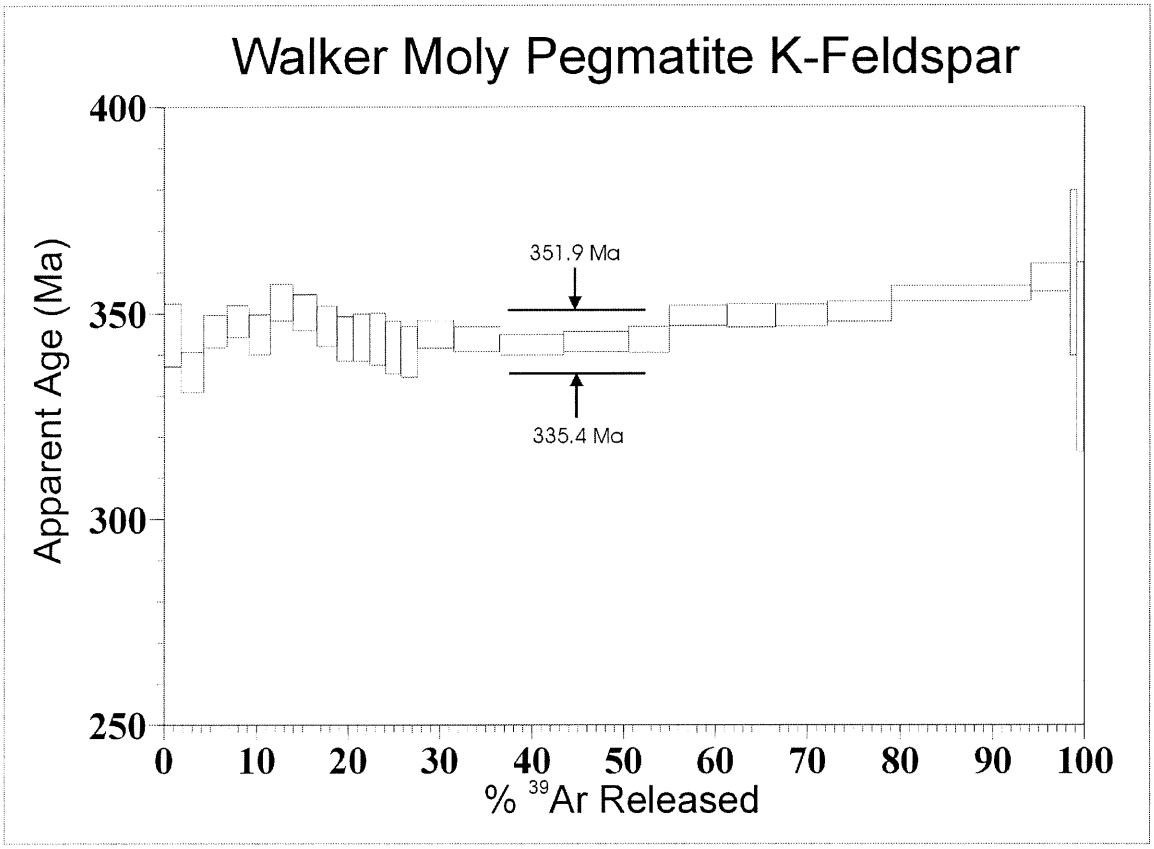

Figure 4.6: Conventional step-heating $^{40}Ar/^{39}Ar$ analysis of SC-9W from previous work. The laser-probe age range is displayed on the spectrum. The total gas age for this sample is 347.9 ± 2.3 Ma.

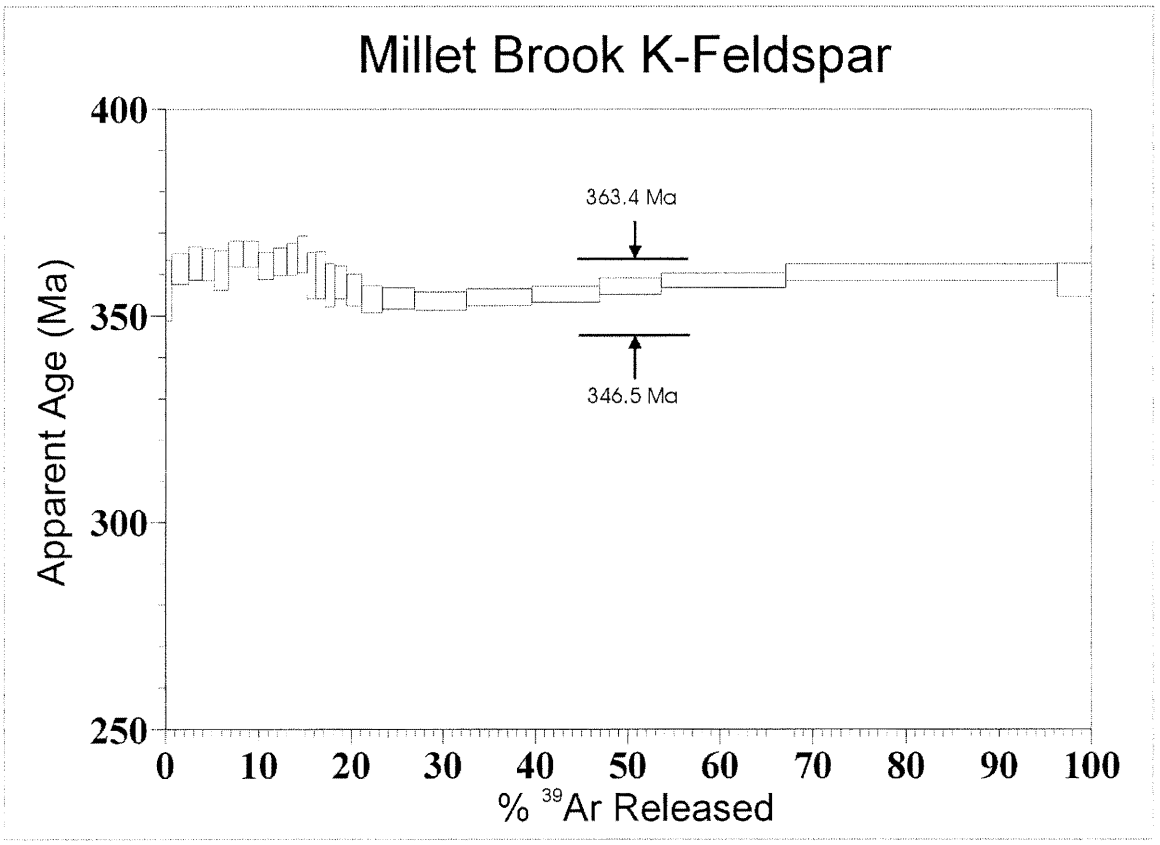

Figure 4.7: Conventional step-heating $^{40}Ar/^{39}Ar$ analysis of DK-MB-99-01from previous work. The laser-probe age range is displayed on the spectrum. The total gas age for this sample is 358.5 ± 2.2 Ma.

4.4 Mineral Petrography

Thin sections were made from the hand samples obtained at each site and examined with the petrographic microscope. Aspects of the feldspars that were noted include the presence and characteristics of the exsolution lamellae, the development of microcline noting occurrence and if it is well developed, and the alteration features of the feldspar. The features that were observed are best presented in the form of a table (see Table 4.1). These features are not uniform over the K-feldspar in thin section. The distribution of exsolution lamellae, the degree of microcline development, the amount of alteration, and the presence of inclusions vary in different areas of the feldspar crystal. This zoning of features is especially present in samples SC-9W and SC-12L. The field of view using the petrographic microscope was determined to be 7 mm. The average thickness of the exsolution lamellae is 0.25 mm. The features observed in the thin sections of feldspar samples are taken as being characteristic of the feldspar samples used for the laser microprobe analysis.

Sample	*Exsolution*	*Development of Microcline*	*Alteration*
Long Lake Mineralized Greisen (SW-LL01)	- There are very minor instances of exsolution lamellae.	Microcline is present although the cross-hatching is difficult to detect.	- Thin section is cloudy indicating kaolinization. - Quartz and muscovite inclusions present (speckley looking in the feldspar). - Muscovite observed within the feldspar resembles the muscovite outside and around the feldspar. This indicates potassic alteration with muscovite, feldspar, and quartz. - Trace amounts of plagioclase are present (plagioclase and K-feldspar usually completely altered to muscovite during greisenization). - There is lots of muscovite around the ksp – characteristic of greisenization.
Walker Moly Pegmatite (SC-9W)	- Lamellae are well-developed and comprise about 20 % of the thin section.	No microcline associated cross-hatching was observed.	- This sample is the most kaolinized of the four samples. This is marked by a cloudy brown characteristic of the thin section. - The feldspar grain boundaries are not sharp and are surrounded by muscovite. - Muscovite filled cracks on the feldspar crystal near the margins. - No inclusions are found within the feldspar crystal.
Long Lake Pegmatite (SC-12L)	- Well-developed lamellae that are mostly irregular and comprise about 30% of the thin section. - The texture of the exsolution lamellae is "patchy" or "wormy" as opposed to straight and relatively parallel. - There are sub-equant pieces of optically clear k-feldspar "islands" within the cloudy lamellae regions that are 0.1 to 0.2 mm in diameter.	No microcline associated cross-hatching was observed.	- Kaolinization is present and indicated as dark brown areas. - Muscovite parallel to cleavages indicating that it is a secondary feature (i.e. cleavage provides a good pathway for fluids) and probably occurred at the same time as kaolinization (cloudy/opaque regions). - The muscovite overprints the K-feldspar. This is observed as the muscovite cutting the exsolution lamellae
Millet Brook Mineralized Fracture (DK-MB-99-01)	- There is less development of exsolution lamellae than in sample SC-12L but they are a similar width. - Albite twins present and are perpendicular to lamellae (twinning within the lamellae). This is plagioclase where displays polysynthetic twinning.	There is good cross-hatching present indicating microcline.	- Smallest amount of kaolinization of the four samples (< 1%). - No secondary muscovite (marked by formation in lamellae and good cleavage). - Trace amounts of primary muscovite are present. They are very irregular and found within intact pieces of K-feldspar. - Primary biotite present.

Table 4.3: General characteristics noted from the petrographic investigation of the thin sections of each of the four samples. Noted are the exsolution lamella, the development of microcline, and the alteration in each of the four K-feldspar samples.

Chapter 5: Summary and Implications

5.1 Discussion and Interpretations

The data that have been presented thus far are summarized in this section and some interpretations are made for each of the four samples and for the mineral deposits in general. Observations made on the core/rim variations are discussed. The differences in the laser-probe age determinations from the step-heating age determinations concerning all four samples are investigated. Discussion and suggestions are made as to the geological significance of these apparent age determinations. Table 5.1 summarizes the results from the laser-probe analysis of samples SW-LL01, SC-9W, SC-12L, and DK-MB-99-01. Table 5.2 summarizes the results of step-heating analysis of SC-9W, SC-12L, and DK-MB-99-01.

	SW-LL01 Long Lake Mineralized Greisen		***SC-9W Walker Moly Pegmatite***		***SC-12L Long Lake Pegmatite***		***DK-MB-99-01 Millet Brook Mineralized Fracture***	
Apparent Mean Age Data (Ma)								
Mean age	260.4 ± 2.8		349.9 ± 3.2		319.6 ± 3.0		355.4 ± 3.5	
Total range	258.7 ± 4.0	265.3 ± 3.9	335.4 ± 5.2	351.9 ± 5.7	279.5 ± 4.7	353.0 ± 6.3	346.5 ± 4.8	363.4 ± 5.3
Rim/Core Age Data (Ma)								
	R = 1	C = 5	R = 13	C = 11	R = 13	C = 12	No Rim/Core Data	
Min age	265.0 ± 4.1	258.7 ± 4.0	335.4 ± 5.2	336.2 ± 4.8	305.2 ± 4.3	279.5 ± 4.7		
Max age	265.0 ± 4.1	265.3 ± 3.9	351.9 ± 5.7	347.1 ± 5.0	344.5 ± 5.3	353.0 ± 6.3		
Mean age	265.0 ± 4.1	260.4 ± 3.2	346.2 ± 4.0	342.7 ± 2.7	327.1 ± 8.3	323.4 ± 20.9		

Table 5.1: Summary of $^{40}Ar/^{39}Ar$ data obtained from the laser-probe analysis of rims and cores from the K-feldspar samples SW-LL01, SC-9W, SC-12L, and DK-MB-99-01.

	SC-9W Walker Moly Pegmatite		*SC-12L Long Lake Pegmatite*		*DK-MB-99-01 Millet Brook Mineralized Fracture*	
Total gas age (Ma)	347.9 ± 2.3		327.0 ± 2.1		358.5 ± 2.2	
Age range (Ma)	342.4 ± 2.4	358.6 ± 3.4	310.6 ± 5.2	346.3 ± 6.4	353.5 ± 2.1	360.4 ± 1.9
% ^{39}Ar	26.8	98.7	30.8	99.2	20.5	96.4
T (degrees C)	940	1250	940	1250	1000	1250

Table 5.2: Summary of conventional step heating results from K-feldspar samples SC-9W, SC-12L, and DK-MB-99-01 including the age range (Ma) of the less discordant portion of each spectrum.

First, the low mean age for the Long Lake greisen SW-LL01 of 260.4 ± 2.8 Ma as determined by the laser-probe stands out from the other mean ages. Even the highest age for a fragment (265.3 ± 3.9 Ma) is lower than any other fragment age. The mineralization is the result of late stage microclinization along a fault caused by potassic fluids as previously stated by O'Reilly et al (1982). However, the mean age for the feldspar of 260.4 ± 2.8 Ma is much lower than the 372 Ma batholith age. This 260 Ma age is not unique in geochronology studies of the SMB. Previous ^{40}Ar/^{39}Ar work on micas has yielded ages of ca. 260 Ma and are believed to be the result of the migration of hot fluids along shear zones (Keppie & Dallmeyer 1995). However, these studies were conducted in the southwestern portion of the SMB so direct comparison is cautioned. No rim/core variations can be determined here because only one of the analyzed fragments was a rim. The apparent age of the rim (265.0 ± 4.1 Ma) is slightly higher than the average apparent age for the cores (260.4 ± 3.2 Ma); however, this is not statistically significant. O'Reilly et al (1982) states that this K-feldspar is the result of microclinization, however, the cross-hatch feature of microcline was difficult to detect in thin section.

The next sample from the same area, Long Lake pegmatite SC-12L, has a notably scattered ^{40}Ar/^{39}Ar laser-probe age plot and an age range that is higher than that determined for the greisen mineralization. The scattered age plot is the result of varying amounts of radiogenic Ar within the grain as well as variations among different feldspar grains. The age spectrum for this sample is also the most discordant of the four samples indicating a large amount of spatial variability of radiogenic Ar. The apparent age from the laser-probe analysis has a scatter range of about 74 Ma whereas the portion of the age spectrum between 30.8 and 99.2 varies by about 36 Ma. The presence of secondary muscovite in this sample indicates that a fluid event has affected the pegmatite at some point over its geologic history. Fluids could have been responsible for the

non-uniform distribution of radiogenic Ar and where they play a significant role in isotopic loss or exchange within minerals (Villa, 1997). If the K-feldspar mineralization from the greisen boulders (SW-LL01) and the pegmatite (SC-12L) are the result of the same event, there has been a significant amount of argon loss experienced by the K-feldspar from the greisen. This may be the result of argon "leakage" in the greisen boulder K-feldspar.

Regarding the Walker Moly pegmatite SC-9W, the low amount of scatter on the laser-probe age plot for the fragments corresponds to the relatively concordant age spectrum from the step heating. The low scatter of the laser plot indicates that the amount of radiogenic Ar is relatively evenly distributed throughout the feldspar as well as evenly distributed among the separate feldspars from which these fragments were obtained. This sample is the most kaolinized of the four samples indicating that the feldspar present in the pegmatite may have been altered at some point during its history assuming that the kaolinite is not a syn-mineralization feature. It is possible that the feldspar has been uniformly altered and has suffered the same amount of Ar loss throughout the crystal.

It may be possible that the absence of inclusions in the SC-9W feldspar accounts for the low variability in apparent age. The laser-probe mean apparent age (349.9 ± 3.2 Ma) is curiously high compared to the SC-12L mean (319.6 ± 3.0 Ma) that has less kaolinization. The total gas age for SC-9W (347.9 ± 2.3 Ma) agrees with the laser-probe mean apparent age within the given range of uncertainty. Also, there is no apparent age difference between feldspar rims and cores (346.2 ± 4.0 and 342.7 ± 2.7, respectively) for this sample.

Finally, the mineralized K-feldspar from Millet Brook has a laser-probe age plot with a low scatter, although this is merely based on six fragments. This is the only sample from the Salmontail Pluton. The age spectrum for this sample is the flattest of the four. Primary minerals are present whereas no secondary minerals are present. With regards to the coupling of the laser with the sample, it is usual that inadequate laser-mineral coupling is an effect of an optically clear mineral grain. Optical-clearness suggests that the K-feldspars have not been altered very much. The low amount of kaolinization and the absence of secondary minerals support this. Altered alkali feldspar would likely contain kaolinite that would not have any significant problem being heated by the laser. Although the sample did contain some kaolinite, there was only a small amount when compared to the other samples. The mean apparent age from the laser-probe (355.4 ± 3.5 Ma) agrees with the total gas age (358.5 ± 2.2 Ma) within error.

From the laser-probe analysis, the maximum apparent age isolated at each location is still under the emplacement age (SC-9W at 351.9 ± 5.7 Ma, SC-12L at 353.0 ± 6.3, and DK-MB-99-01 at 363.4 ± 5.3 Ma). One possible suggestion is that the system could have remained open and radiogenic argon was not retained until after about 360 Ma. However, the base of the overlying sediments of the Horton Group has been determined to be 355 Ma (Martel et al. 1993). These sediments are located to the northeast of the New Ross area (Figure 2.1). Therefore, the New Ross area of the SMB was exhumed by that time and completely cooled. However, it is possible that hot fluids could have been focussed up fault zones during the Carboniferous, which would result in partially reset feldspar ages. This explanation involving fluid activity during the Carboniferous and Early Permian times is used to explain the low isotopic age determinations in the East Kemptville-Yartmouth area (Keppie & Dallmeyer 1995).

5.3 Conclusions

1. Although the Nd-YAG laser is typically not used for the analysis of K-feldspar on account of poor coupling, there were no significant problems encountered in this study. This may be because the samples were not "pure" K-feldspar. The presence of impurities likely affected the K-feldspar optical properties and facilitated coupling.

2. Laser-probe analysis of K-feldspar from Long Lake, Walker Moly, and Millet Brook produce age ranges which correlate approximately with the respective spectral age range however the mineralization age of 372 Ma was not isolated. The scatter of the apparent age data from the laser-probe analysis in SC-12L and DK-MB-99-01 (ca. 74 and 17 Ma, respectively) is on the order of double the amount of scatter produced from the age spectra (ca. 36 and 7 Ma, respectively). This may reflect the averaging tendency of the step-heating analysis where spatial variations in age in these K-feldspars may be relatively large.

3. No significantly apparent age variation was observed in the rims or cores of each of the samples where this was tested. Thus, variable apparent ages are not related to the proximity to the outer margins of the feldspar crystals for these samples (namely SC-9W and SC-12L).

5.3 Recommendations for Further Research

First, it may be of interest to investigate how each type of K-feldspar mineralogical characteristic affects the obtained age. This aspect was not well assessed in this thesis where the features observed in thin section were merely assumed to exist in the analyzed samples. Only one thin section per sample was described. It may be of interest to identify the texture and mineralogical features of each of the K-feldspar fragments for a given sample. Perhaps dating feldspar fragments or regions of the feldspars that have a high degree of microcline development, contain a large proportion of exsolution lamellae, or are highly altered would bring some understanding to the age variations that exist with these feldspars.

Secondly, it is possible to analyze fragments that are much smaller than those used in this study. The present instrumentation at Dalhousie University is capable of accurately dating mineral fragments that release a tenth the amount of argon that was released from the fragments in this study. Therefore, a much higher resolution study of these feldspars is possible.

References

Attendorn, H. –G. & Bowen, R. N. C. 1997. *Radioactive and Stable Isotope Geology*. Chapman & Hall, London.

Carruzzo, S., Kontak, D. J., & Clarke, D. B. In prep. Granite-hosted mineral deposits of the New Ross area, South Mountain Batholith, Nova Scotia, Canada: P, T, and X constraints of fluids using fluid inclusion thermometry and decrepitate analysis.

Chatterjee, A. K. & Strong, D. F. 1984. Discriminant and factor analysis of geochemical data from granitoid rocks hosting the Millet Brook uranium mineralization, South Mountain Batholith, Nova Scotia. *Uranium* **1**, 289-305.

Clarke, D. B., MacDonald, M. A., & Tate, M. C. 1997. Late Devonian mafic-felsic magmatism in the Meguma Zone, Nova Scotia. *In* The nature of magmatism in the Applachian Orogen. *Edited by* A. K. Sinha, J. B. Whalon, and J. P. Holgan. Geological Society of America, Memoir **191**, pp. 107-127.

Dickin, A. P. 1995. *Radiogenic Isotope Geology*. Cambridge University Press. pages 245-274.

Harrison, T. M. 1990. Some observations on the interpretation of feldspar $^{40}Ar/^{39}Ar$ results. *Chemical Geology (Isotope Geoscience Section)* **80**, 219-229.

Keppie, J. K. & Dallmeyer, R. D. 1995. Late Paleozoic collision, delamination, short-lived magmatism, and rapid denudation in the Meguma terrane (Nova Scotia, Canada): constraints from $^{40}Ar/^{39}Ar$ isotopic data. *Canadian Journal of Earth Sciences* **32**, 644-659.

Lee, J. K. W., Onstott, T. C., Cashman, K. V., Cumbest, R. J., & Johnson, D. 1991. Incremental heating of hornblende in vacuo: implications for $^{40}Ar/^{39}Ar$ geochronology and the interpretation of thermal histories. *Geology* **19**, 872-876.

MacDonald, M. A. In press. Geology of the South Mountain Batholith, Nova Scotia. Nova Scotia Department of Natural Resources Open File Report.

MacDonald, M. A., Horne, R. J., Corey, M. C., & Ham, L. J. 1992. An overview of recent bedrock mapping and follow-up petrological studies of the South Mountain Batholith, Southwestern Nova Scotia, Canada. *Atlantic Geology* **28**, 7-28.

Martel, A. T., McGregor, D. C., & Utting, J. 1993. Stratigraphic significance of Upper Devonian and Lower Carboniferous miospores from the type area of the Horton Group, Mova Scotia. *Canadian Journal of Earth Sciences* **30**, 1091-1098.

McDougall, I. & Harrison, T. M. 1999. *Geochronology and Thermochronology by the $^{40}Ar/^{39}Ar$ Method*. Second Edition. Oxford University Press. 269 pp.

O'Reilly, G. A. 1992. Petrographic and geochemical evidence for a hypogene origin of granite-hosted, vein-type Mn mineralization at the New Ross Mn deposits, Lunenburg County, Nova Scotia, Canada. *Economic Geology* **87**, 1275-1300.

O'Reilly, G. A., Farley, E. J., & Charest, M. H. 1982. Metasomatic-Hydrothermal Deposits of the New Ross-Mahone Bay Area, Nova Scotia. Nova Scotia Department of Mines and Energy, Paper **82-2**.

Parsons, I., Brown, W. L., & Smith, J. V. 1999. $^{40}Ar/^{39}Ar$ thermochronology using alkali feldspars: real thermal history or mathematical mirage of microtexture? *Contrib Mineral Petrol* **136**, 92-110.

Sampson, S. D. and Alexander, E. C., Jr. 1987. Calibration of the interlaboratory $^{40}Ar/^{39}Ar$ dating standard, MMHb-1. *Chem. Geol. (Isot. Geosci. Section)* **66**, 27-34.

Schenk, P. E. 1995. Meguma Zone. *In* Geology of the Appalachia-Caledonian Orogen in Canada and Greenland. *Edited by* H. Williams. Geological Survey of Canada, Geology of Canada, No. 6, Chapter 3, pp. 261-277. (Also Geological Society of America, The Geology of North America, Vol F-1.)

Villa, I. M. 1997. Isotopic closure. *Terra Nova* **10**, 42-47.

Wartho, J. –A., Kelley, S. P., Brooker, R. A., Carroll, M. R., Villa, I. M., & Lee, M. R. 1999. Direct measurement of Ar diffusion profiles in a gem-quality Madagascar K-feldspar using the ultra-violet laser ablation microprobe (UVLAMP). *Earth and Planetary Science Letters* **170**, 141-153.

Williams, H. & Hatcher, R.D. 1982. Suspect terranes and accretionary history of the Appalachian orogen. *Geology* **10**, 530-536.

Windley, B. F. 1984. *The Evolving Continents*. Third Edition. Wiley.

Appendix 1: $^{40}Ar/^{39}Ar$ Laser-Probe Data

SW-LL01 K-FELDSPAR ARGON SUMMARY

SPOT NO.	CODE NO.	mV 39	AGE (Ma) $\pm 2\sigma$	% ATM	37/39	36/40	39/40	% IIC
1	B78-21	934.1	258.7 ± 4	15.4	.06	.000523	.013882	.01
2	B78-17	755.7	261.7 ± 4	15.4	.01	.000521	.013718	0
3	B78-13	376.3	265 ± 4.1	13.7	0	.000465	.013804	0
4	B78-20	2154.9	257 ± 4.1	17.3	.01	.000588	.013657	0
5	B78-22	594.5	259.7 ± 4	14.8	.01	.000501	.013926	0
6	B78-25	1302.4	265.3 ± 3.9	12.3	.01	.000416	.014017	0

AGE UNCERTAINTIES AT 2σ LEVEL, INCLUDING ERROR IN J

MEAN AGE(SPOTS 1 - 6)= 260.4 ± 2.8 Ma (2σ UNCERTAINTY, INCLUDING ERROR IN J)

J = .002533 ± .000025 (.9 %)

37/39, 36/40 AND 39/40 Ar RATIOS ARE CORRECTED FOR MASS SPECTROMETER DISCRIMINATION, INTERFERING ISOTOPES AND SYSTEM BLANKS

% IIC - INTERFERING ISOTOPES CORRECTION

SC-12L K-FELDSPAR ARGON SUMMARY

SPOT NO.	CODE NO.	mV 39	AGE (Ma) ±2σ	% ATM	37/39	36/40	39/40	% IIC
1	B79-1	236	329.3 ± 4.9	7.1	.01	.000241	.011571	0
2	B79-16	800.1	298.2 ± 4.2	10.3	.01	.000349	.012448	0
3	B79-17	464.9	323.3 ± 4.4	5.9	.01	.0002	.011961	0
4	B79-2	240.7	324.7 ± 4.7	7.6	.01	.000257	.011692	0
5	B79-3	341.2	333.5 ± 4.7	6.7	0	.000229	.011456	0
6	B79-18	159.3	339.3 ± 5.3	5	.01	.000171	.011446	0
7	B79-19	596.4	345.5 ± 4.6	5.3	0	.00018	.011191	0
8	B79-4	211.3	317.8 ± 4.8	8	.01	.000273	.011907	0
9	B79-5	261.1	332.9 ± 4.9	9.1	.01	.000309	.011187	0
10	B79-6	464.7	305.2 ± 4.3	8.3	.01	.000282	.012403	0
11	B79-20	337	321.5 ± 4.4	5.5	.01	.000187	.012082	0
12	B79-21	734.6	283.6 ± 4.5	17.6	.01	.000597	.012065	0
13	B79-7	173.9	323.5 ± 5.1	9.4	.01	.00032	.0115	0
14	B79-8	178.9	335.6 ± 5.1	6.6	.01	.000224	.011395	0
15	B79-9	218.3	332.9 ± 6.4	6.9	.01	.000236	.011451	0
16	B79-10	183.6	344.5 ± 5.3	6.4	.01	.000216	.011099	0
17	B79-22	127.8	349.1 ± 5.6	3.8	.02	.000128	.011242	0
18	B79-23	162.8	347.6 ± 5.2	2.6	.01	.000089	.01143	0
19	B79-26	257.4	279.5 ± 4.7	17.8	.02	.000602	.012237	0
20	B79-11	175.4	312.6 ± 5.3	10.7	.02	.000363	.011769	0
21	B79-12	188.1	325.2 ± 5	6.5	.01	.00022	.011807	0
22	B79-13	182.8	334.9 ± 5	5.4	.01	.000185	.01156	0
23	B79-24	105.4	353 ± 6.3	3.3	0	.000113	.011158	0
24	B79-25	118.1	309.2 ± 5.7	12.6	.01	.000428	.011654	0
25	B79-29	269.7	331.4 ± 4.7	6.6	0	.000223	.011556	0

AGE UNCERTAINTIES AT 2σ LEVEL, INCLUDING ERROR IN J

MEAN AGE(SPOTS 1 - 25)= 319.6 ± 3 Ma (2σ UNCERTAINTY, INCLUDING ERROR IN J)

J = .002496 ± .000025 (1 %)

37/39, 36/40 AND 39/40 Ar RATIOS ARE CORRECTED FOR MASS SPECTROMETER DISCRIMINATION, INTERFERING ISOTOPES AND SYSTEM BLANKS

% IIC - INTERFERING ISOTOPES CORRECTION

SC-9W K-FELDSPAR ARGON SUMMARY

SPOT NO.	CODE NO.	mV 39	AGE (Ma) ±2σ	% ATM	37/39	36/40	39/40	% IIC
1	B80-12	574.3	340.4 ± 4.7	7.2	0	.000245	.011224	0
2	B80-13	469.2	351.3 ± 4.9	8.8	0	.000297	.01066	0
3	B80-15	281	349.7 ± 4.8	3.1	.01	.000107	.011375	0
4	B80-26	320.4	346.1 ± 5	10.3	.01	.000351	.01065	0
5	B80-27	384.2	343.3 ± 4.9	8.7	0	.000295	.010945	0
6	B80-28	1651.9	336.2 ± 4.8	9.2	.01	.000311	.011138	0
7	B80-9	334	343.3 ± 4.9	8.1	.01	.000275	.011013	0
8	B80-10	255.3	348.6 ± 4.9	4.9	.01	.000168	.011202	0
9	B80-25	690.7	343.9 ± 4.8	9.7	0	.00033	.010796	0
10	B80-24	791.4	340.4 ± 4.7	9.1	.01	.000309	.010994	0
11	B80-11	198.2	351.9 ± 5.7	13.1	.01	.000446	.010128	0
12	B80-8	138.1	347.8 ± 5.4	3.7	.02	.000128	.011368	0
13	B80-5	122	350 ± 6.2	10.4	.02	.000353	.01051	0
14	B80-6	242.4	349.1 ± 5	6.8	.01	.000233	.010958	0
15	B80-7	175	347.2 ± 5.6	11.1	.1	.000377	.010518	.01
16	B80-21	231.3	342.2 ± 5.1	8.9	.01	.000301	.010958	0
17	B80-22	293.7	344.3 ± 5	8.5	.01	.00029	.010925	0
18	B80-23	144.2	343.4 ± 5.5	4.5	.02	.000154	.011439	0
19	B80-2	103.1	340.1 ± 6.2	8.3	0	.000282	.011102	0
20	B80-3	158.5	345.5 ± 5.8	9	.01	.000307	.010823	0
21	B80-4	186.1	335.4 ± 5.2	9.1	.01	.000308	.011175	0
22	B80-18	196.4	337.3 ± 5.1	5.1	0	.000175	.011591	0
23	B80-19	256.6	347.1 ± 5	6.7	.01	.00023	.011039	0
24	B80-29	282	345.5 ± 4.9	6.3	0	.000216	.011146	0

AGE UNCERTAINTIES AT 2σ LEVEL, INCLUDING ERROR IN J

MEAN AGE(SPOTS 1 - 24)= 342.9 ± 3.2 Ma (2σ UNCERTAINTY, INCLUDING ERROR IN J)

J = .002514 ± .000025 (.9 %)

37/39, 36/40 AND 39/40 Ar RATIOS ARE CORRECTED FOR MASS SPECTROMETER DISCRIMINATION, INTERFERING ISOTOPES AND SYSTEM BLANKS

% IIC - INTERFERING ISOTOPES CORRECTION

DK-MB-99-01 K-FELDSPAR ARGON SUMMARY

SPOT NO.	CODE NO.	mV 39	AGE (Ma) $\pm 2\sigma$	% ATM	37/39	36/40	39/40	% IIC
1	B82-17	448.5	355.2 ± 4.7	1.7	0	.00006	.011513	0
2	B82-26	265.8	354.4 ± 4.8	2.2	.01	.000077	.011481	0
3	B82-25	103.8	358.4 ± 6.2	1	.01	.000035	.011489	0
4	B82-18	168.9	358.7 ± 5.4	2.9	.01	.000099	.011258	0
5	B82-22	242.5	346.5 ± 4.8	1.2	0	.000043	.011893	0
6	B82-16	212.1	363.4 ± 5.3	1.3	.01	.000045	.011278	0

AGE UNCERTAINTIES AT 2σ LEVEL,INCLUDING ERROR IN J

MEAN AGE(SPOTS 1 - 6)= 355.4 ± 3.5 Ma (2σ UNCERTAINTY,INCLUDING ERROR IN J)

J = .002552 ± .000025 (.9 %)

37/39,36/40 AND 39/40 Ar RATIOS ARE CORRECTED FOR MASS SPECTROMETER DISCRIMINATION,INTERFERING ISOTOPES AND SYSTEM BLANKS

% IIC - INTERFERING ISOTOPES CORRECTION

Appendix 2: $^{40}Ar/^{39}Ar$ Step-Heating Data

SC-12L K-FELDSPAR ARGON SUMMARY

T°C	mV 39	% 39	AGE (Ma) ±1σ	% ATM	37/39	36/40	39/40	% IIC
550	49.8	2	294.4 ± 5.6	3.7	.01	.000127	.012276	0
580	78.2	3.2	320 ± 3.9	4.2	0	.000143	.011144	0
610	88.1	3.6	329.6 ± 3.5	2.7	0	.000094	.010952	0
640	74.8	3	334.3 ± 3.6	1.1	0	.000037	.010969	0
700	153.2	6.3	345.2 ± 2.9	9.8	0	.000332	.00965	0
730	80.7	3.3	331.5 ± 3.3	.9	0	.000033	.011085	0
760	51.5	2.1	324.9 ± 4.9	.6	.01	.000022	.011377	0
790	37.8	1.5	323.5 ± 6.8	.2	0	.000009	.011492	0
820	33.8	1.3	319.6 ± 7.3	.3	0	.000011	.011644	0
850	31.7	1.3	315.5 ± 7.9	1.1	.01	.00004	.011711	0
880	37.1	1.5	309.9 ± 7.1	4.9	.01	.000167	.011481	0
910	42.2	1.7	306.4 ± 6.4	4.8	.01	.000164	.011627	0
940	57.3	2.3	310.6 ± 5.2	7.3	.01	.000249	.011143	0
970	80.5	3.3	311.1 ± 4.2	8.7	.01	.000295	.010949	0
1000	113.2	4.6	313.6 ± 3.6	9.2	.01	.000313	.010785	0
1025	133.8	5.5	315.9 ± 2.9	9.5	0	.000322	.010667	0
1050	137.3	5.6	314.8 ± 2.9	9.3	.01	.000317	.010726	0
1075	135.3	5.5	319.7 ± 3	7.2	.01	.000246	.010789	0
1100	138.6	5.7	323.7 ± 2.7	4.9	0	.000167	.010914	0
1125	176.5	7.2	327.4 ± 2.3	3.7	0	.000125	.010918	0
1150	238.8	9.8	332.5 ± 2	3.1	0	.000106	.010791	0
1200	393.2	16.1	343.5 ± 1.8	2.4	0	.000081	.010493	0
1250	44.7	1.8	346.3 ± 6.4	6.6	0	.000225	.009974	0
1350	14.7	.6	342.3 ± 20.6	31.6	0	.001079	.007416	0
1450	5.7	.2	329 ± 79.6	77	.04	.002623	.002599	0

TOTAL GAS AGE = 327 ± 2.1 Ma

J = .002255 ± 1.1275E-05 (.5 %)

37/39,36/40 AND 39/40 Ar RATIOS ARE CORRECTED FOR MASS SPECTROMETER DISCRIMINATION,INTERFERING ISOTOPES AND SYSTEM BLANKS

% IIC - INTERFERING ISOTOPES CORRECTION

SC-9W K-FELDSPAR ARGON SUMMARY

T°C	mV 39	% 39	AGE (Ma) ±1σ	% ATM	37/39	36/40	39/40	% IIC
550	39.4	1.8	344.7 ± 7.6	15.5	.02	.000526	.008994	0
580	52	2.4	335.8 ± 4.8	4.3	.01	.000145	.010485	0
610	54.9	2.5	345.7 ± 3.9	2.5	0	.000087	.010336	0
640	51.6	2.3	348.1 ± 3.9	1.8	0	.000061	.010341	0
670	49.9	2.3	344.8 ± 4.9	4.9	0	.000166	.010118	0
700	52.6	2.4	352.6 ± 4.4	3.4	0	.000118	.010018	0
730	56.1	2.5	350.2 ± 4.3	3.5	0	.00012	.010086	0
760	48	2.2	346.9 ± 4.8	4.2	0	.000143	.010125	0
790	38.5	1.7	343.8 ± 5.3	3.4	0	.000118	.010306	0
820	38.7	1.7	344.1 ± 5.7	3.2	0	.000109	.010324	0
850	37.2	1.7	343.7 ± 6.3	4.4	0	.000151	.010206	0
880	35.9	1.6	341.7 ± 6.3	6	.01	.000203	.010105	0
910	38.4	1.7	340.7 ± 6.1	5.6	.01	.000193	.010174	0
940	86.1	3.9	344.9 ± 3.3	5	0	.000171	.010092	0
970	107.4	4.9	343.7 ± 3	5.2	0	.000176	.010115	0
1000	150.6	6.9	342.4 ± 2.4	5.2	0	.000177	.010154	0
1025	152.3	7	343.1 ± 2.4	5.1	0	.000172	.010144	0
1050	95.7	4.4	343.6 ± 3.1	4.9	0	.000166	.010152	0
1075	136.1	6.3	349.4 ± 2.4	2.9	0	.0001	.010168	0
1100	114.3	5.2	349.4 ± 2.8	3.9	0	.000132	.010068	0
1125	121.1	5.6	349.5 ± 2.6	2.8	0	.000095	.01018	0
1150	149.1	6.9	350.4 ± 2.4	2.7	0	.000094	.010154	0
1200	325.8	15	354.8 ± 1.8	2.3	0	.00008	.010055	0
1250	93.1	4.3	358.6 ± 3.4	6.3	0	.000215	.009537	0
1350	14.9	.6	359.7 ± 20	36	0	.001222	.006511	0
1450	16.4	.7	339.2 ± 22.9	55.7	0	.00189	.004799	0
1500	1.6	0	412.4 ± 623	94	.1	.003187	.000523	.01

TOTAL GAS AGE = 347.9 ± 2.3 Ma

J = .002239 ± 1.1195E-05 (.5 %)

37/39,36/40 AND 39/40 Ar RATIOS ARE CORRECTED FOR MASS SPECTROMETER DISCRIMINATION,INTERFERING ISOTOPES AND SYSTEM BLANKS

% IIC - INTERFERING ISOTOPES CORRECTION

DK-MB-99-01 K-FELDSPAR ARGON SUMMARY

T°C	mV 39	% 39	AGE (Ma) ±1σ	% ATM	37/39	36/40	39/40	% IIC
500	1.5	0	301.4 ± 107	-72.8	.34	-.002734	.023843	.05
550	18.3	.6	356.1 ± 7.3	.4	.02	.000016	.010336	0
600	56.5	1.8	361.3 ± 3.6	2.8	0	.000097	.009901	0
625	43.3	1.4	362.6 ± 3.9	.4	.01	.000015	.010111	0
650	40.2	1.3	362.4 ± 3.8	.4	.01	.000015	.010119	0
675	45.9	1.5	360.9 ± 4.7	4.1	.01	.000141	.009781	0
700	47.7	1.5	364.8 ± 3	.2	.01	.000009	.010059	0
725	49.5	1.6	364.8 ± 3.1	.2	.01	.000007	.010063	0
750	50.4	1.6	362 ± 3.2	.7	.01	.000025	.010097	0
775	43.5	1.4	363 ± 3.3	.4	0	.000014	.0101	0
800	35.8	1.1	363.6 ± 3.8	.3	.01	.000012	.010091	0
825	31.3	1	364.8 ± 4.4	.2	.01	.00001	.010065	0
850	27	.8	359.6 ± 5.5	1.1	.01	.000039	.01014	0
875	31.8	1	359.8 ± 5.7	2.8	.01	.000096	.009958	0
900	31.1	1	357.3 ± 5.2	2.8	0	.000096	.010035	0
925	39.7	1.3	358 ± 3.9	1.5	.01	.000053	.010141	0
950	49.6	1.6	356.2 ± 3.8	1.7	0	.000059	.010173	0
975	67.8	2.2	354 ± 3.2	2.3	0	.000079	.010178	0
1000	108.9	3.5	354.2 ± 2.5	2.4	0	.000083	.010155	0
1025	171	5.6	353.5 ± 2.1	2.2	0	.000076	.010194	0
1050	216.2	7	354.4 ± 2	2.3	0	.00008	.010154	0
1075	221	7.2	355.2 ± 1.9	2	.01	.00007	.010161	0
1100	205.8	6.7	357.1 ± 1.9	1.8	.01	.000062	.010126	0
1150	410.2	13.4	358.5 ± 1.7	1.5	0	.000052	.010109	0
1250	892	29.2	360.4 ± 1.9	2.2	0	.000076	.00998	0
1450	111.8	3.6	358.6 ± 4	27.1	0	.000917	.007484	0

TOTAL GAS AGE = 358.5 ± 2.2 Ma

J = .002258 ± 1.129E-05 (.5 %)

37/39,36/40 AND 39/40 Ar RATIOS ARE CORRECTED FOR MASS SPECTROMETER DISCRIMINATION,INTERFERING ISOTOPES AND SYSTEM BLANKS

% IIC - INTERFERING ISOTOPES CORRECTION